SECTION I: STRUCTURAL ANALYSIS

INTRODUCTION

Structural work for this thesis has been concentrated in the Coffs Harbour Block where preliminary results have already been reported (Korsch 1973), and in the Rockvale Block, where a large area of the Girrakool Beds has been overturned. An attempt will be made to outline the geological structures present and to determine the deformational history for the Rockvale - Coffs Harbour Region.

In a typical structure analysis it is customary to divide a region into homogeneous domains after having determined the orientation of the structural elements throughout the region. This method has been described in detail by Turner and Weiss (1963). Most earlier studies have been carried out on extremely small areas of well-exposed rocks enabling very detailed mapping and delineation of the history of very complex areas. In the Rockvale - Coffs Harbour region it is apparent that the usual methods of structural analysis cannot be rigorously applied because of the size of the region, lack of access to parts of it, poor or very limited exposure in most parts and considerable weathering in places. Hence the structural analysis presented here has been attempted on a large regional scale to try to outline some of the features of the structural history of the whole region. Sampling has been inadequate both in the amount of data presented for certain areas and also in the distribution of the sampling points. In many places in the discussion this will be obvious, but at the same time, it has been possible to piece together a unified structural history for the Rockvale - Coffs Harbour region.

The major aims of this structural analysis have been:

(1) To describe the mesoscopic structures produced by the deformations, and to determine their distribution.

(2) To determine the number and sequential development of the several generations of structures present, particularly in the Rockvale Block.

(3) To attempt to define major structural elements and to describe the structural evolution of the tectonic blocks.

(4) To assess the age of the tectonism and attempt to relate it to regional metamorphism and plutonic activity within the region.

(5) To relate the deformational episodes in each block to adjoining areas and to observe the relationship of the Rockvale - Coffs Harbour region with the remainder of the New England area.

The mesoscopic structures and deformational history of each tectonic block are described separately and then a regional synthesis and correlation between blocks is attempted.

NOMENCLATURE

All structural data measured in the field were recorded onto a Structural Analysis Data Sheet (Type 3) designed by Dr. K.L. Burns of Division of Mineral Physics, CSIRO. An earlier version of the data sheet has been described by Burns *et al.* (1969, p.45). The format of this data sheet and descriptions of the computer programs used in the structural analysis are given in Appendix II. The data sheet relies on the principle that all structural elements can be grouped into seven varieties:

1. **SF** - folded surface
2. LF - noncomposite lineation in SF
3. SG - generated surface
4. CL (SF, SG) - composite lineation
5. AX (SF, SG) - fold axis
6. AS (SF, SG) - axial surface
7. ES (SF, SG) - enveloping surface

The styles and ages of the elements, given as a two digit code, are listed in Appendix II.

EXAMPLES OF NOMENCLATURE

For simplification the names of structural elements are abbreviated, examples being FOLIATION to FOLN, FOLD AXIS to FAX, and LINEATION to LIN. The abbreviations are accompanied by the two digit qualifiers mentioned above (and in Appendix II), as in the following examples:

1. FOLN 31 - axial plane cleavage in pelitic rocks.

2. FAX (13, 31) Style 21 - fold axis produced by the intersection of FOLN 13 (lithological alternation in thick beds) and FOLN 31 (axial plane cleavage in pelites). Style is 21 (sharp, closed, parallel fold with distinct hinge which is rectilinear).

3. LIN NCOM SF 13 Style 30 - noncomposite lineation measured in foliation 13 (lithological alternation in thick beds). Style is 30 (flute or groove casts where relation to the fold axis is either not known or irrelevant).

The nomenclature described above, along with nomenclature based on Turner and Weiss (1963, p.131) is used throughout this thesis. A nomenclature in the style of Turner and Weiss groups all structures produced during one deformational period together, e.g. D_2 is the second deformational period; S_2 is the second surface developed; L_2 is the lineation produced by the intersection of S_2 and an earlier S-surface; B_2 is the fold axis produced by the deformation of an earlier S-surface and having S_2 as its axial surface. Hence in general, D = deformational period; S = S-surface; L = lineation, B = fold axis. So is used for original bedding. Lineations and fold axes are often written L(Sx x Sy) and B^{Sy}_{Sx} where Sx is the older (often folded) S-surface, and Sy is the axial surface to the fold or the younger S-surface.

The above nomenclature has been applied to the three tectonic blocks in the Rockvale - Coffs Harbour region, so that D_1, S_1, FOLN 13 (and so on) occur in every block, but each block is regarded as a separate entity and therefore S_1 (or any other element) present in one block need not be the same age as the S_1 (or the element of the same notation) present in another block. Hence D_1 and D_2 in one block may well be distinct deformations and may not be correlatives of the D_1 and D_2 observed in an adjacent block.

CHAPTER 1: THEORETICAL ASPECTS OF FOLDING

During field work and subsequent interpretation a number of problems relating to the geometry of the mesoscopic structures were encountered and could not be solved by the explanations of earlier workers for similar structures elsewhere. Solutions to the problems have been devised and tested. It has been necessary to develop some quantitative measures to describe the style of folds.

PROBLEM 1

Korsch (1968, 1973) described a progressive decrease in the inter-limb angles of mesoscopic folds, from open in the north to tight in the south, in the Woolgoolga district. This decrease suggested an increase, towards the south, in the intensity of the deformation which produced the folds. The geometries of these folds have to be considered before any attempt to explain the kinematics or dynamics can be made.

Van Hise (1896) subdivided folds into two geometrical groups which he termed parallel and similar. There has been opposition to the term "parallel" because parts of adjacent form surfaces can be parallel in both groups of folds. Consequently, a number of later writers (e.g. de Sitter 1956, Turner and Weiss 1963) have referred to parallel folds as concentric folds. However Mertie (1940) has shown that the term concentric is unsuitable, and the term "parallel" is used here.

By utilizing dip isogons devised by Elliott (1965), J.G. Ramsay has been able to classify folds into three geometrical types. A complete discussion has been provided by Ramsay (1967, pp.363-372) and will not be duplicated here. Mesoscopic folds from the Rockvale - Coffs Harbour region cannot be classified adequately by Ramsay's method. For example, Fold B (Fig. 29) approximates to a class 1B fold but contains some elements of a class 1A fold whereas Fold C (Fig. 29) contains elements of a class 1C and elements of a class 2 fold. Korsch (1973) has shown that mesoscopic folds in the coarser-grained sediments have an approximately parallel fold geometry. However the intervening finer-grained layers have been less competent during deformation and consequently are difficult to describe in terms of either of the above classifications. Hence the need arises for a more adequate method for the quantification of the geometry of folds.

PROBLEM 2

Korsch (1973, Fig. 2B) showed that the plunge of D_1 fold axes changes systematically from subhorizontal to steeply plunging, from north to south in the Woolgoolga district. The problem of explaining a change in the plunge of fold axes has been discussed by many workers. Lillie (1960, 1962a, 1962b, 1963) and Lillie and Gunn (1964) have described steeply plunging folds from the Southern Alps of New Zealand. Lillie (1961) proposed two mechanisms for the growth of steeply plunging folds: the rotation of partly formed folds with continued steepening of the limbs, or the development of new folds on limbs that were already steeply dipping because of an earlier fold episode. He did not envisage any simple rotation of earlier formed folds and attributed the folding to a strike-slip regime associated with the Alpine Fault. Waterhouse (1972), also working in the Southern Alps, invoked the formation of schuppen to steepen the dip and tectonically thicken the sequence, followed by two periods of folding associated with a strike-slip regime in a subduction zone to produce the steeply plunging folds.

Borradaile (1972) invokes a progressive irrotational constrictive deformation to explain variably oriented folds in the Scottish Highlands. However these folds have a large variation in trend coupled with only a slight variation in the plunge of the fold axes. Crosby and Link (1972) invoke stress reorientation to explain curved and steeply plunging fold axes in Wyoming. Roy (1972) interprets variable plunges and trends of the axes of upright folds in western India as a product of the interference of two periods of folding. Garnett and Brown (1973) prefer a single period of protracted heterogeneous strain to produce a progressive change from subhorizontal to steeply plunging mineral-clast lineations and hinge lines, in a constant vertical axial surface, in Canada.

All of the above explanations for a change in the plunge of fold axes, while possibly suitable for the areas where the change was described, are not applicable to the change in the Coffs Harbour Block where the mesoscopic structures present a simple geometrical picture (see Chapter 2). There is no evidence to indicate a widespread second period of folding and hence the explanations of Roy and Lillie are not applicable. The explanations outlined by Crosby and Link, and Garnett and Brown are considered to invoke stresses of too complex a nature to explain the relatively simple geometry of the mesoscopic structures in the Coffs Harbour Block. Consequently a new explanation will be outlined in an attempt to solve this problem.

PROBLEM 3

When a group of geologists approach an outcrop showing features such as those illustrated in Plates 3 and 4 they immediately recognise the presence of a cleavage. In the case of the illustrated cleavage if the geologists did not know the relationship to the axial surface, the majority would probably call it a fracture cleavage because the planes are only statistically parallel and not truly parallel as for a slaty cleavage. However on learning that the cleavage was parallel to the axial surfaces of the mesoscopic folds many of the geologists would redefine the structure as a slaty cleavage. In brief, the criteria used to distinguish fracture from slaty cleavage are not clear, and in fact some authors state that one cleavage can pass into the other, indicating a common origin (e.g. Ramsay 1967, p.406).

What criteria can be used to distinguish between fracture cleavage and slaty cleavage? Previous authors have varied widely in their choice of criteria to define the cleavage but most use one or more of the following properties:

1. The orientation of the cleavage with respect to the axial surface. Is the cleavage parallel to the axial surface? Are there two cleavage orientations?
2. Is there a preferred orientation of minerals, particularly the phyllosilicates?
3. The spacing criteria used by Chidester (1962). Are the cleavage planes spaced or "continuous"? Is the cleavage plane continuous or is it disrupted through a bed or layer?

Table 1 summarises criteria used by a number of authors to define the differences between slaty and fracture cleavage. From this table it can be concluded that criteria A, C and E refer mainly to slaty cleavage and that B, D and F refer to fracture cleavage. The cleavage illustrated in Plate 3 has criterion A (slaty cleavage) and criteria D and F (fracture cleavage). Hence the criteria outlined above are not sufficient to classify this cleavage definitely as a slaty or fracture cleavage. The problem is to establish criteria whereby the two cleavages can be distinguished, and to determine the mechanism of their formation.

Table 1: Properties used by selected authors to distinguish between slaty and fracture cleavage

Reference	Slaty Cleavage	Fracture Cleavage	Reference	Slaty Cleavage	Fracture Cleavage
Sorby 1857	C	D	Hills 1963	C	D,F
Becker 1893	C,E	-	Crook 1964	-	A,D,F
Van Hise 1896	C	B,D	de Sitter 1964	C	F
Leith 1905	A,C	B,D	Whitten 1966	A,C,E	D
Mead 1940	A,C	B,D	Dennis 1967	A,E	D
Broughton 1946	C	D	Ramsay 1967	E	F
Wilson 1946	A,C	B,D,F	Carson 1968	A,C,E	A,B,D
Billings 1954	A,C,E	B,D	Dieterich 1969	A,C	A,B,D
Gonzalez-Bonorino 1960	-	D	Williams *et al.* 1969	A,C	-
Knill 1960	A,C	A,B,D	Powell 1969	A,C,E	-
Rickard 1961	C	D	Clark 1970	A,C	-
Wilson 1961	A,C	A,B,D	Braddock 1970	A,C	-
Chidester 1962	E	A,B,D,F	Moench 1970	A,C,E	-
Maxwell 1962	A,C	B,D,F	Price & Hancock 1972	-	B,D,F
Fyson 1962	A,C,D	B,C,D	Moore & Geigle 1974	A,C	-
Turner & Weiss 1963	C	D	Geiser 1974	-	B,C,F

Key

Property	Description
A	Cleavage is parallel to the axial plane
B	Cleavage is oblique to axial plane, may have two orientations
C	Cleavage defined by preferred orientation of minerals
D	No preferred orientation of minerals exists
E	Cleavage is continuous through a bed
F	Cleavage is spaced or disrupted through a bed

THEORETICAL ASPECTS OF FOLDS AND FOLDING

In attempting to solve the three problems outlined above some theoretical aspects of folds and folding have been considered. This chapter will concentrate on the geometry of folds, with reference to both single fold layers and fold stacks and trains. They will be described under several headings following Fleuty (1964):

1. Component parts of folds;
2. Dimensions of folds;
3. Shapes and styles of folds (morphology);
4. Attitudes of folds, and relationship of the marker surface (form surface) to the axial surface;

and,

5. Description of and derivation of cleavages, particularly axial plane cleavages.

1. COMPONENT PARTS OF FOLDS

Fleuty (1964) provided an important paper on the description of folds and much of his terminology is used here with modifications. It is set out briefly below because the literature on folds is in a state of flux and expansion, which could lead to confusions of meaning.

The hinge zone (Wilson 1961) varies from a surface with constant curvature to a surface with a line of maximum curvature (the hinge line). The term axial surface (Challinor 1945) is preferred to the term axial plane because not all axial surfaces are planar. Clark and McIntyre (1951, p.595) defined the axial surface as "the locus of the hinges of all beds forming the fold" and this is followed here although it cannot be applied rigorously to folds lacking distinct hinge lines. The modal bisecting surface, defined as the surface bisecting the limbs of a fold, can easily be determined on a stereographic projection. In symmetrical folds the modal bisecting surface is coincident with the axial surface.

The fold axis is defined by McIntyre (1950, p.331) and Clark and McIntyre (1951) as "the nearest approximation to the line which moved parallel to itself generates the (fold) surface". Hence following this definition it can be seen that the attitude of the fold axis is determined

more reliably by the use of a stereographic projection than by direct measurement of a hinge line in the field. Fold axes for mesoscopic folds in the Coffs Harbour - Rockvale region have been determined by both methods. The enveloping surfaces (Turner and Weiss 1963) are defined as the two limiting surfaces of a fold train, between which the train oscillates.

2. DIMENSIONS OF FOLDS

Three scales adopted here follow Turner and Weiss (1963, p.15) and are: microscopic, mesoscopic and macroscopic. Most of the folds with which this section is concerned are on the mesoscopic scale, but the theoretical analyses can be applied readily to folds on any scale.

It is possible to describe the dimensions of periodic folds by three elements: amplitude (A), wavelength (λ) and interlimb angle (θ), (Fleuty 1964). The wavelength (Fig. 2) is the length of a periodic unit, measured from one point to the corresponding point on the next fold, and the amplitude is half the perpendicular distance between the two enveloping surfaces. The interlimb angle is "the minimum angle between the limbs, as measured in the profile plane" (Fleuty 1964, p.469). This parameter does not define the absolute scale of the fold but can describe the degree of acuteness of the fold.

Matthews (1958) has provided a method whereby asymmetrical folds can be described by the short and long limb lengths and axial plane separations for both the short and long limbs. Nevertheless, the terms outlined earlier are preferred because of their relative simplicity. It is assumed that for symmetrical folds the two limbs are of equal length and the axial surface is normal to the enveloping surface and that for asymmetrical folds the limbs are of unequal lengths and the axial surface is not normal to the enveloping surface.

Assumptions in this study are that for buckle folding the length of the neutral surface (L) within a marker horizon has remained constant throughout the deformation (Ramsay 1967) and that A, λ and θ have changed systematically. For slip folding it is assumed that λ remains constant and L, A and θ change systematically.

In the general case it is possible to derive equations for the calculation of λ, A and percent shortening (V, defined as original length minus final wavelength, expressed as a percentage of the original length).

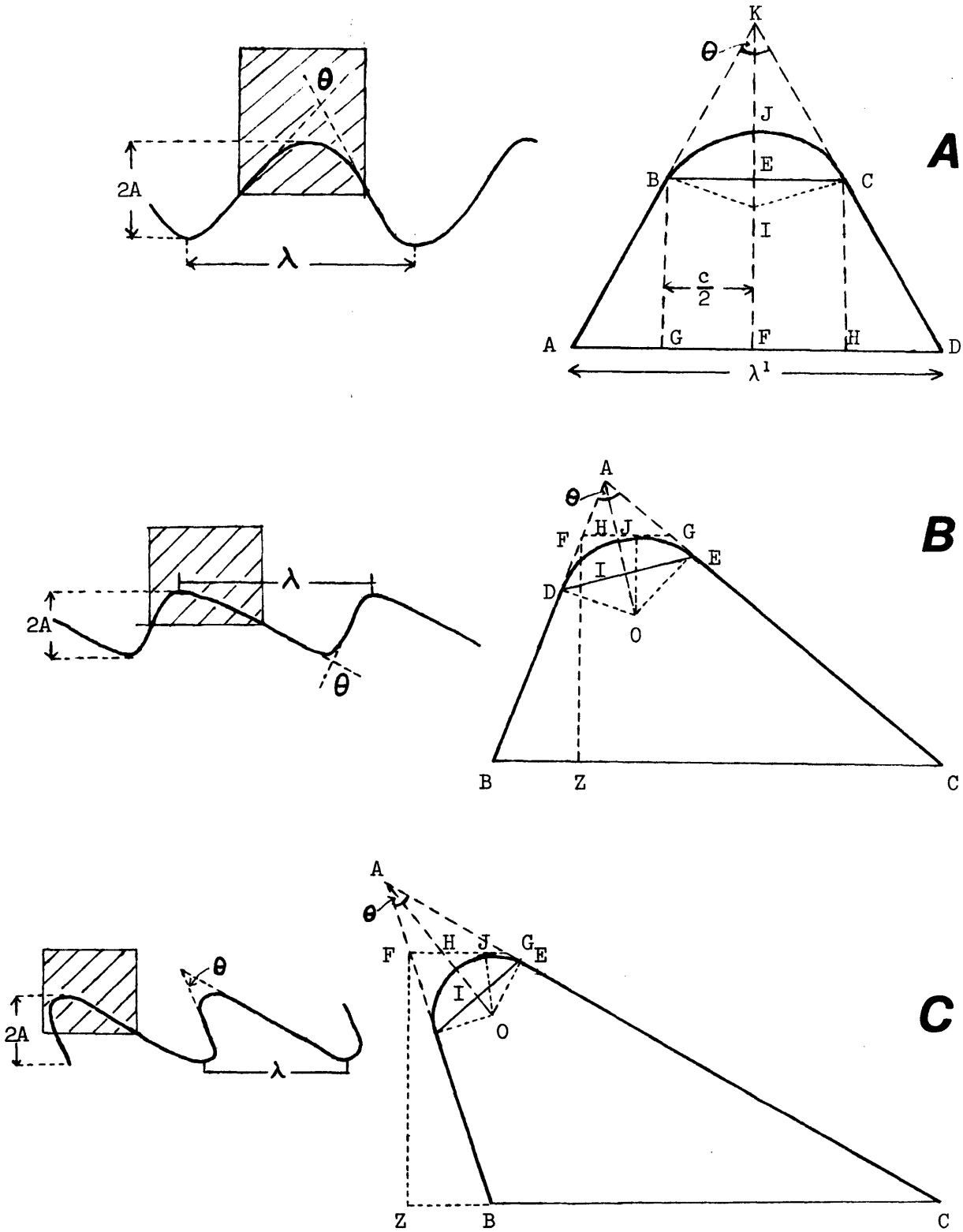

Fig. 2: Dimensions and components of symmetrical folds (A) and asymmetrical folds (B and C).

Furtak and Richter (1967) have provided equations for determining V for angular, circular and rounded folds using the following parameters:

(1) α = angle between tangent to limb and chord of the arc,

(2) a = length of straight portion of limb produced to the point of intersection with the straight portion of the other limb, and,

(3) n = length of straight portion of the limb.

The method presented here differs from that of Furtak and Richter in the choice of the three variables. For symmetrical folds the following variables are used:

(1) θ = interlimb angle,

(2) c = chord length, that is, length of chord subtending the arc in the fold, and,

(3) f = halflength of fold, that is, twice the length of the limb of a fold from the point of inflection to the chord, plus the length of arc.

c and f can be measured in the profile plane in the field using a flexible tape measure, or in the laboratory from a specimen or photograph using a flexible ruler.

It is considered that the parameters described here are easier to measure in the field or derive from photographs or sections measured in the profile plane than are those of Furtak and Richter. The subsequent calculations are more tedious. However it has been possible to computerise the data, and program SHORTNIN provides values of λ, A and V for differing values of θ and C in symmetrical folds (see Appendix II). C is defined as the ratio of the chord length to the half fold length, that is, $C = \frac{c}{f}$, where $f = \frac{L}{2}$ and L is the initial length of the fold, often taken as unity.

SYMMETRICAL FOLDS

For symmetrical folds $0 \leqslant C \leqslant 1$ and $0° \leqslant \theta \leqslant 180°$

Using Fig. 2A,
Let radius of arc of circle ($\overline{IB}$ and $\overline{IC}$) = r and length of AB = s

Using trigonometry,

In Δ ABG, $\sin\left(\frac{\theta}{2}\right) = \frac{(\lambda' - c)}{2s}$

$$\therefore \lambda' = c + 2s \sin\left(\frac{\theta}{2}\right) \qquad \text{---------- (1)}$$

Now f = 2s + arclength

$\therefore$ 2s = f - arclength

and $2s = f - \left[\frac{180 - \theta}{180}\right] \cdot \Pi r$ ---------- (2)

From Δ EBI, $\cos\left(\frac{\theta}{2}\right) = \frac{c/2}{r}$

$$r = \frac{c}{2 \cos\left(\frac{\theta}{2}\right)} \qquad \text{---------- (3)}$$

Substitute (3) into (2)

$$2s = f - \left[\frac{180 - \theta}{180}\right] \cdot \frac{c\Pi}{2 \cos\left(\frac{\theta}{2}\right)} \qquad \text{---------- (4)}$$

Substitute (4) into (1)

$$\lambda' = c + \left\{f - \left[\frac{180 - \theta}{180}\right] \cdot \frac{\Pi c}{2 \cos\left(\frac{\theta}{2}\right)}\right\} \cdot \sin\left(\frac{\theta}{2}\right)$$

$$\therefore \lambda' = c + f.\sin\left(\frac{\theta}{2}\right) - \left[\frac{180 - \theta}{180}\right] \cdot \Pi c. \tan\left(\frac{\theta}{2}\right)$$

From Fig. 2A,

$$\lambda' = \tfrac{1}{2} \lambda$$

$$\therefore \quad = 2 \lambda'$$

and,

$$\boxed{\lambda = 2c + 2f.\sin\left(\frac{\theta}{2}\right) - \left[\frac{180 - \theta}{180}\right] . \Pi c. \tan\left(\frac{\theta}{2}\right)}$$

Now $A = BG + (JI - EI)$

$$= s.\cos\left(\frac{\theta}{2}\right) + \left[r - r\sin\left(\frac{\theta}{2}\right)\right]$$

$$= s.\cos\left(\frac{\theta}{2}\right) + r.\left[1 - \sin\left(\frac{\theta}{2}\right)\right] \qquad \text{---------- (5)}$$

From (2), $s = \frac{f - \left(\frac{180 - \theta}{180}\right).\Pi r}{2}$

From (3), $r = \frac{c}{2 \cos (\frac{\theta}{2})}$

Substituting into (5),

$$A = \left[f - (\frac{180 - \theta}{180}) \cdot \frac{\Pi c}{2 \cos (\frac{\theta}{2})} \right] \cdot \cos (\frac{\theta}{2}) + \frac{c}{2 \cos (\frac{\theta}{2})} \cdot \left[1 - \sin (\frac{\theta}{2}) \right]$$

$$\boxed{A = \frac{f}{2} \cdot \cos (\frac{\theta}{2}) - \frac{(180 - \theta)\ \Pi c}{720} + \frac{c}{2 \cos (\frac{\theta}{2})} - \frac{c}{2} \cdot \tan (\frac{\theta}{2})}$$

To determine percent shortening, $V = (L - \lambda) \times 100\%$

Since $C = \frac{c}{f}$, three types of folds can be defined:

(1) $C = 0$

The fold is angular (chevron) in style. Hence $\lambda = \sin (\frac{\theta}{2})$ and $A = \frac{1}{4} \cos(\frac{\theta}{2})$ because $f = \frac{L}{2}$.

For folds where $C = 0$,

(a) as the interlimb angle θ decreases from 180° to 0°, the wavelength decreases in ratio $\sin (\frac{\theta}{2})$ from 1 to 0.

(b) as θ decreases from 180° to 0°, the amplitude increases in ration $\frac{1}{4} \cos(\frac{\theta}{2})$ from 0 to 0.25.

(c) as θ decreases, V increases from 0 to 100% in ration $[1 - \sin (\frac{\theta}{2})] \times 100$.

(2) $0 < C < 1$

This is the general case for rounded symmetrical folds (paraboloidal) folds. A special case occurs when $\theta = 0$ and the folds are semi-circular (de Sitter 1958). For these folds $\lambda = 2C = 0.64$, $A = 0.16$ and $V = 36\%$, and the folds are in the class 1B (parallel folds) of Ramsay (1967). With further compressive strain the fold shape originally formed by buckling is modified and becomes a flattened parallel fold (class 1C fold).

(3) $C = 1$

For this case $\lambda = C$ and $\theta = 180°$. In other words, the folded surface remains a straight line and has not been buckled, or deformed in any way.

Results computed by program SHORTNIN have been graphed for differing values of C and θ (Fig. 3). For pure circular-arc parallel folds $\theta = 0$ and $V = 36\%$. This plots as a point on the graphs. It is not possible to

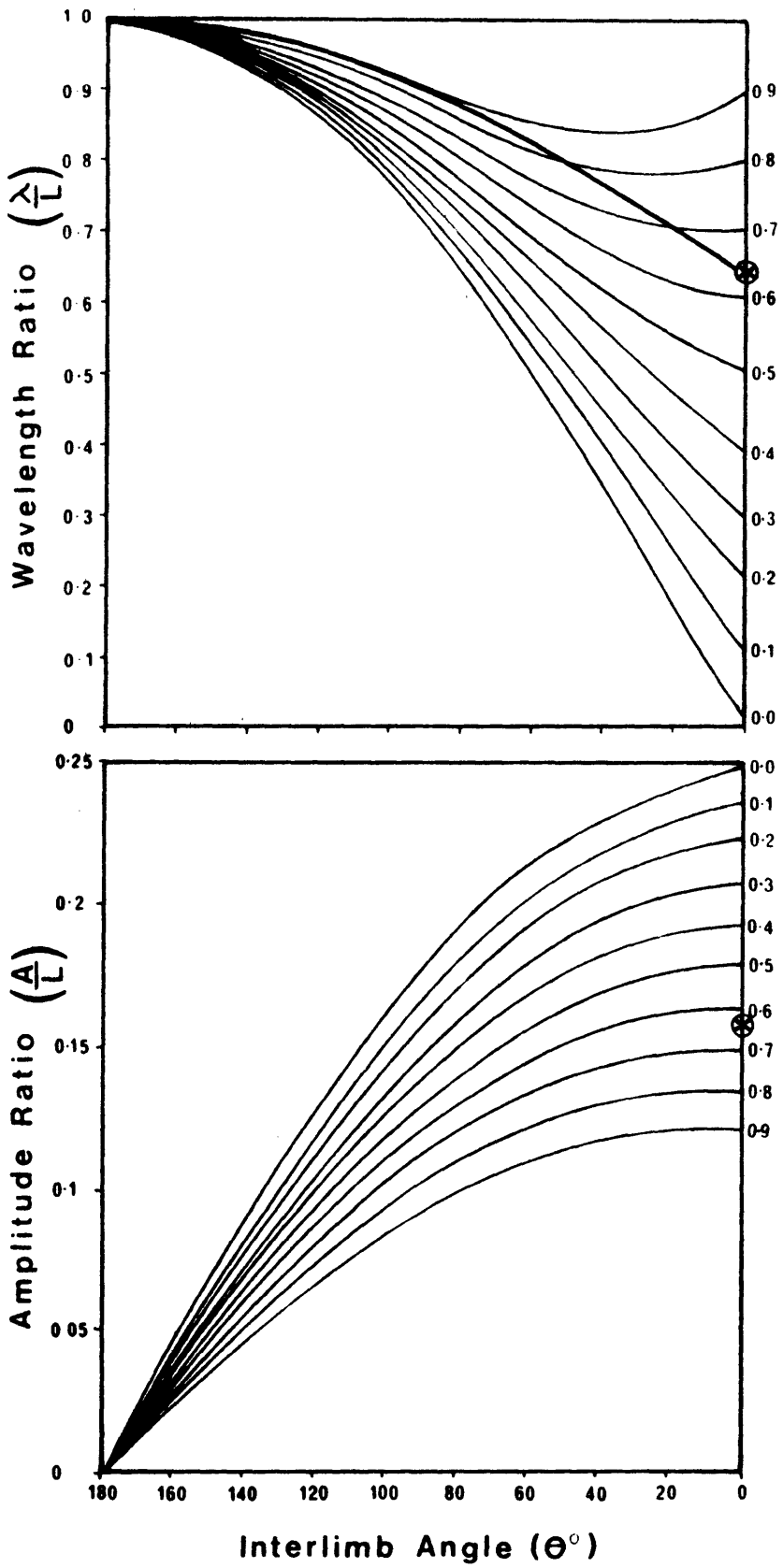

Fig. 3: Values of $\frac{\lambda}{L}$ and $\frac{A}{L}$ versus θ, for differing curves of C. —— in $\frac{\lambda}{L}$ v. θ graph is curve where C = λ. ⊗ is position of pure circular arc parallel folds.

delineate other classes of folds of the Ramsay classification on the graphs, because the graphs are produced for folded surfaces and not for a single layer or group of layers. An alternative to the graphs in Figure 3, utilizing $2A/\lambda$ versus V has been used by Currie *et al.* (1962).

The formula for λ, A and V can be applied not only to buckle and flattened folds but also to folds produced by the slip mechanism and other periodic symmetrical folds, providing the interlimb angle, chord length and half fold length are known. For similar folds λ, A and θ remain constant in a stack. However for paraboloidal parallel folds A and θ vary up and down the stack as λ remains constant.

ASYMMETRICAL FOLDS

For periodic asymmetrical folds, from Figs. 2B and C,

$< BAC = \theta$, $DB = s$, $EC = 1$, $DE = c$.

In Δ DOI, $r = \dfrac{c}{2 \cos (\frac{\theta}{2})}$ ---------- (1)

In Δ ADI, $AD = AE = \dfrac{c}{2 \tan (\frac{\theta}{2})}$ ---------- (2)

Hence $AB = s + \dfrac{c}{2 \tan (\frac{\theta}{2})}$,

and $AC = 1 + \dfrac{c}{2 \tan (\frac{\theta}{2})}$

Using cosine rule,

$BC^2 = AB^2 + AC^2 - 2AB.\ AC.\ \cos \theta$

$$= \left[s + \frac{c}{2 \tan (\frac{\theta}{2})}\right]^2 + \left[1 + \frac{c}{2 \tan (\frac{\theta}{2})}\right]^2 - 2 \cos \theta \left[s + \frac{c}{2 \tan (\frac{\theta}{2})}\right] \cdot \left[1 + \frac{c}{2 \tan (\frac{\theta}{2})}\right]$$

let $BC^2 = EXP1$

$$EXP1 = s^2 + 1^2 + c. \left[\frac{1 - \cos \theta}{\tan (\frac{\theta}{2})}\right] \cdot (s + 1) + \frac{c^2(1 - \cos \theta)}{2 \tan^2 (\frac{\theta}{2})} - 2s.1.\cos \theta$$

$$BC = \sqrt{EXP1} = \frac{\lambda}{2}$$

$$\boxed{\lambda = 2. \sqrt{EXP1}}$$

Using sine rule,

$$\frac{BC}{\sin\theta} = \frac{AC}{\sin B}$$

$$\sin B = \frac{\left[1 + \frac{c}{2\tan(\frac{\theta}{2})}\right] \cdot \sin\theta}{\sqrt{EXP1}}$$

hence $$B = \arcsin\left\{\frac{\left[1 + \frac{c}{2\tan(\frac{\theta}{2})}\right] \cdot \sin\theta}{\sqrt{EXP1}}\right\}$$

In Δ AFH, $< AHF = (180 - (\frac{\theta}{2}) - B)$

In Δ HJO, $< JOH = (\frac{\theta}{2}) + B - 90)$

$$OH = \frac{c}{2\cos(\frac{\theta}{2}).\cos(\frac{\theta}{2} + B - 90)}$$

In Δ ADO, $$AO = \frac{c}{2\cos(\frac{\theta}{2}).\sin(\frac{\theta}{2})}$$

$$\text{Length AH} = AO - OH$$

$$= \frac{c}{2\cos(\frac{\theta}{2}).\sin(\frac{\theta}{2})} - \frac{c}{2\cos(\frac{\theta}{2}).\cos(\frac{\theta}{2} + B - 90)}$$

In AFH, using sine rule,

$$\frac{AF}{\sin(180 - \frac{\theta}{2} - B)} = \frac{AH}{\sin B}$$

Let $AF = EXP2$

$$EXP2 = \frac{\sin(180 - (\frac{\theta}{2}) - B)}{\sin B} \cdot \left[\frac{c}{2\cos(\frac{\theta}{2}).\sin(\frac{\theta}{2})} - \frac{c}{2\cos(\frac{\theta}{2}).\cos(\frac{\theta}{2} + B - 90)}\right]$$

$$\text{Length BF} = AB - AF$$

$$= s + \frac{c}{2\tan(\frac{\theta}{2})} - EXP2$$

In FBZ, $FZ = A$

$$A = \sin B \cdot \left[s + \frac{c}{2\tan(\frac{\theta}{2})} - EXP2\right]$$

Because of the complex nature of these formulae for periodic asymmetric folds, the quickest method of deriving results is to computerise the formulae and insert data for various folds. When s = 1, the limbs are of equal length and the fold is symmetrical. A chord ratio, defined as $C = \frac{c}{s + 1 + \frac{c.(180 - \theta)}{2 \cos (\frac{\theta}{2})}}$ can be used to define three types of folds:

(1) C = 0, the folds are asymmetrical angular folds.

(2) $0 < C < 1$, this is the general case and the folds are rounded asymmetrical folds.

(3) C = 1, here C = total length of fold and is a straight line, $\theta = 180°$ and no folding has occurred.

3. SHAPE (OR STYLE) OF FOLDS

The shape (or style) of a fold is taken as the shape of the folded layer or layers in the profile plane (normal to the fold axis). Fold shapes have been divided into cylindrical and non-cylindrical by authors such as Mertie (1959) and Fleuty (1964). A cylindrical fold has been defined by Stockwell (1950) as a curved geological surface generated by a straight line (the fold axis) which is moved parallel to itself through space. Fleuty (1964) summarises terms which have been used to describe fold shapes and claims that shapes can be described by the nature of the hinge zone, form of the limbs, and relationship of two adjoining fold surfaces.

The most useful way of describing fold shape, up to the present, has been by thickness parameters, T and t (Ramsay 1962) and dip isogons (Elliott 1965). Ramsay (1967) presents a comprehensive coverage of these two topics and his work has been extended by Hudleston (1973 a, b, c), particularly for single layer folds. In the following discussion additional techniques will be described which might help to elucidate the style of single fold layers, fold trains and fold stacks.

Hansen (1971) rejected the use of amplitude and wavelength particularly for asymmetrical folds and substituted the terms height (H) and width (W). These have orientations different from those of the amplitude and wavelength. A ratio H/W was used by Hansen to express quantitatively the relative amount that a layer has been folded (or doubled) back on itself. This ratio has been adopted in principle, and in this thesis is modified to the A/λ ratio, which

ranges from zero (θ = 180°), through 1 (λ = A) towards infinity ($\theta \rightarrow 0$, $C \rightarrow 0$). Hence as A/λ varies from 0 towards ∞, the flattening of the fold increases.

Ramsay (1967, p.350) defined a parameter, P_1, to describe the shapes of folds in cross section, to avoid a confusion of folds with the same interlimb angles but differing shapes. His parameter is:

$$P_1 = \frac{\text{length of projection of limbs for the join of } i_1\ i_2}{\text{length of projection of hinge zone on join of } i_1\ i_2}$$

(where i_1 and i_2 are inflection points on the limbs).

For angular folds $P_1 \rightarrow \infty$, whereas for pure circular-arc parallel folds $P \rightarrow 0$. His parameter is similar to the ration A/λ used here.

Using the values of λ, A, C and θ calculated by SHORTNIN it is possible to construct a series of symmetrical folds of varied styles in the profile plane (Fig. 4A). On this diagram two fields of folds can be delineated:

(1) For a constant θ there is a spectrum of folds varying from angular towards rounded for differing values of C between 0 and 1. Two special cases occur when C = 0 (angular folds) and C = 1 (straight line) and the value of C determines the degree of <u>roundness</u> of a fold.

(2) For a constant C there is a spectrum from open to isoclinal folds with differing values of θ between 0 and 180°. Two special cases occur when θ = 180° (straight line) and θ = 0 (isoclinal folds). The interlimb angle determines the degree of <u>acuteness</u> of a fold.

For certain values of θ and C a relationship exists where the chord length is greater than the wavelength (see Figs. 3 and 4A). This unusual field where $C > \lambda$ may be accounted for by one of the following explanations:

(1) the situation is not real, the folds cannot form, and hence the field is a forbidden one.

(2) Fracturing, shearing or thrusting may occur to compensate for the greater length of the chord. This is illustrated schematically in Figure 4B and may help to explain the shearing in the limbs of many folds. Shearing is more likely to occur when the value of θ is approaching zero, but may occur for larger values of θ when C approaches L in value (Fig. 3). For similar folds (e.g. Dennis 1967, Fig. 22) as θ approaches zero there is considerable attenuation of the limbs and consequently

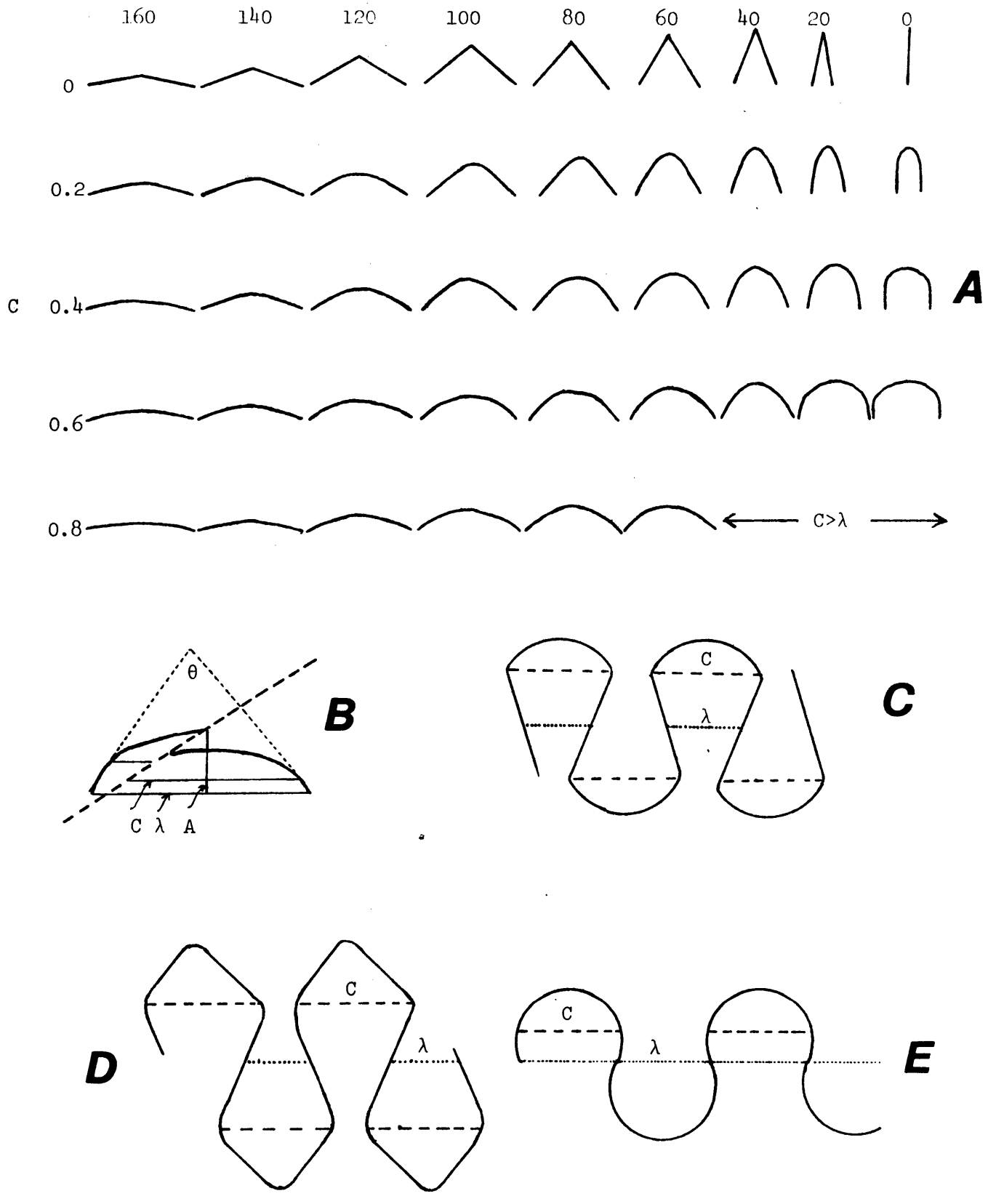

Fig. 4 A: Styles of symmetrical folds for changing values of C and θ, using λ and A values calculated by SHORTNIN.

B-E: Possible explanations for the unusual situation C>λ. See text (pp. 15-16) for full explanation.

shearing frequently develops. De Sitter (1964, Fig. 121) shows a parallel fold in which fracturing may have occurred as a response to these conditions.

(3) The folds may be an unusual shape (see Fig 4C, D, E). Figure 4C consists of a series of straight limbs separated by circular arcs and obeys the definition of a fold by Weiss (1959), as a curved arrangement of a set of originally parallel s-surfaces. The fold in Figure 4D contains multiple hinges between straight limbs. Hence it is possible that the $C>\lambda$ field is occupied by folds which have multiple inflection points and multiple hinges. In cylindrical folds the multiple hinges in one fold would presumably be parallel. However an axial surface would be present for each stack of hinges, and in the theoretical folds that are illustrated the two axial surfaces have different orientations. For these symmetrical folds the axial surfaces are perpendicular. An example of this type of fold is the fan fold (Billings 1954, Fig. 28B). Salt domes and other diapirs may also fall into this category.

(4) A special case of Figure 4C occurs when limbs do not occur and the folds consist of a series of constant curvature circular arcs greater than a semi-circle (Fig. 4E and cf. Willis and Willis 1929, Fig. 23). This style may also be that of ptygmatic folds as indicated by Johnson (1970, p. 170, Fig. 4.17.C). Because of the continuous curvature of the folds it is difficult to define an interlimb angle.

It is possible that the folds described above (Fig. 40-E) only occur in interference patterns resulting from superposed deformations, or resulting from cross folding during a single period of folding (e.g. compare Fig. 4C and 4D with Fig. 1 of O'Driscoll, 1962).

DIP ISOGONS

As mentioned previously, Ramsay (1967) classified folds into three classes using the layer thickness method (Ramsay 1962) and dip isogons (Elliott 1965). Four profiles of theoretical folds along with dip isogon patterns and graphs of t and T versus α for different layers in the folds are presented in Figures 5 and 6.

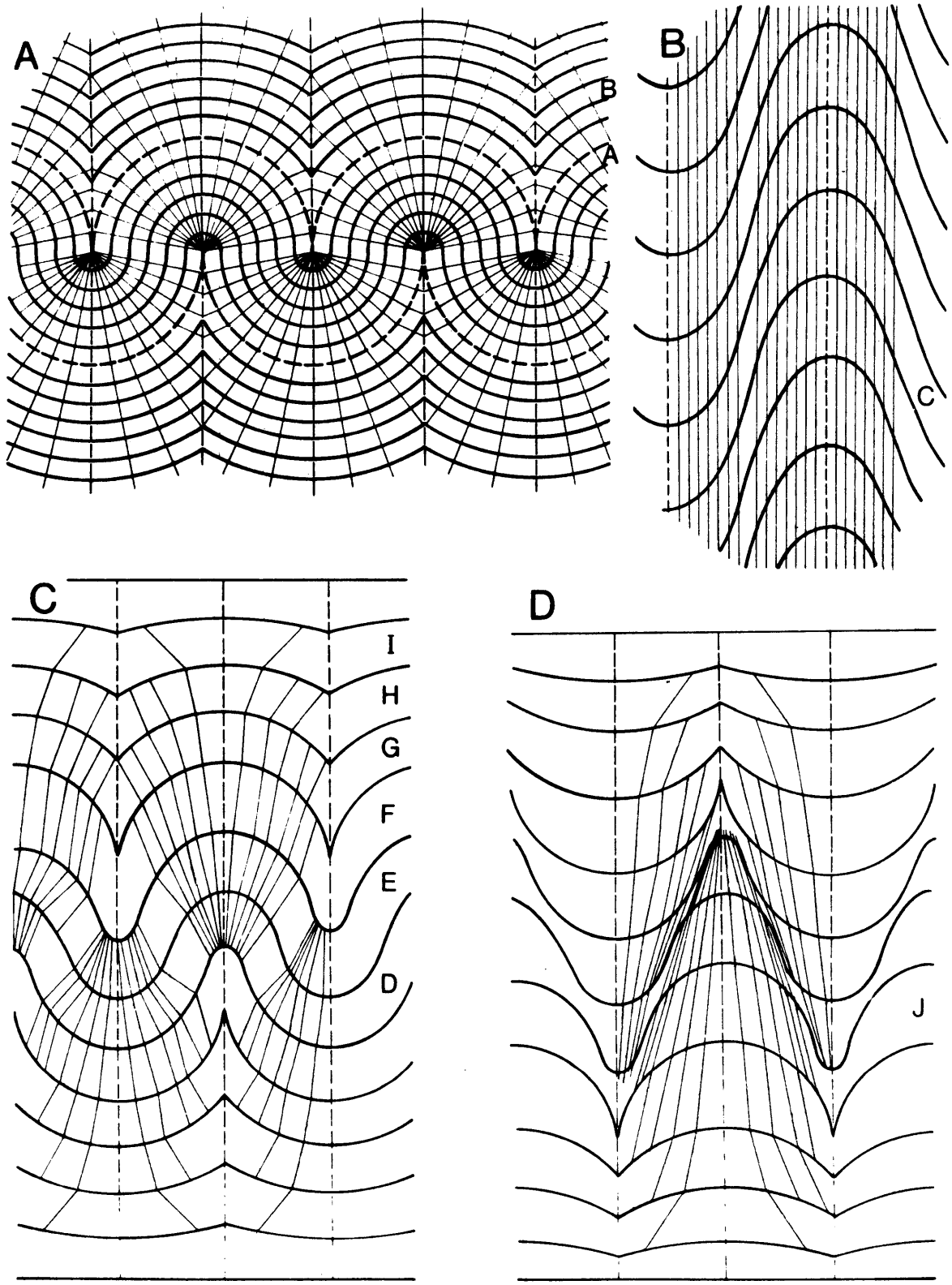

Fig. 5: Dip isogons drawn at 10^{o} intervals for profiles of theoretical folds. A - idealised pure circular-arc parallel fold, B - idealised similar folds, C - idealised paraboloidal parallel folds, D - theoretical class 3 folds.

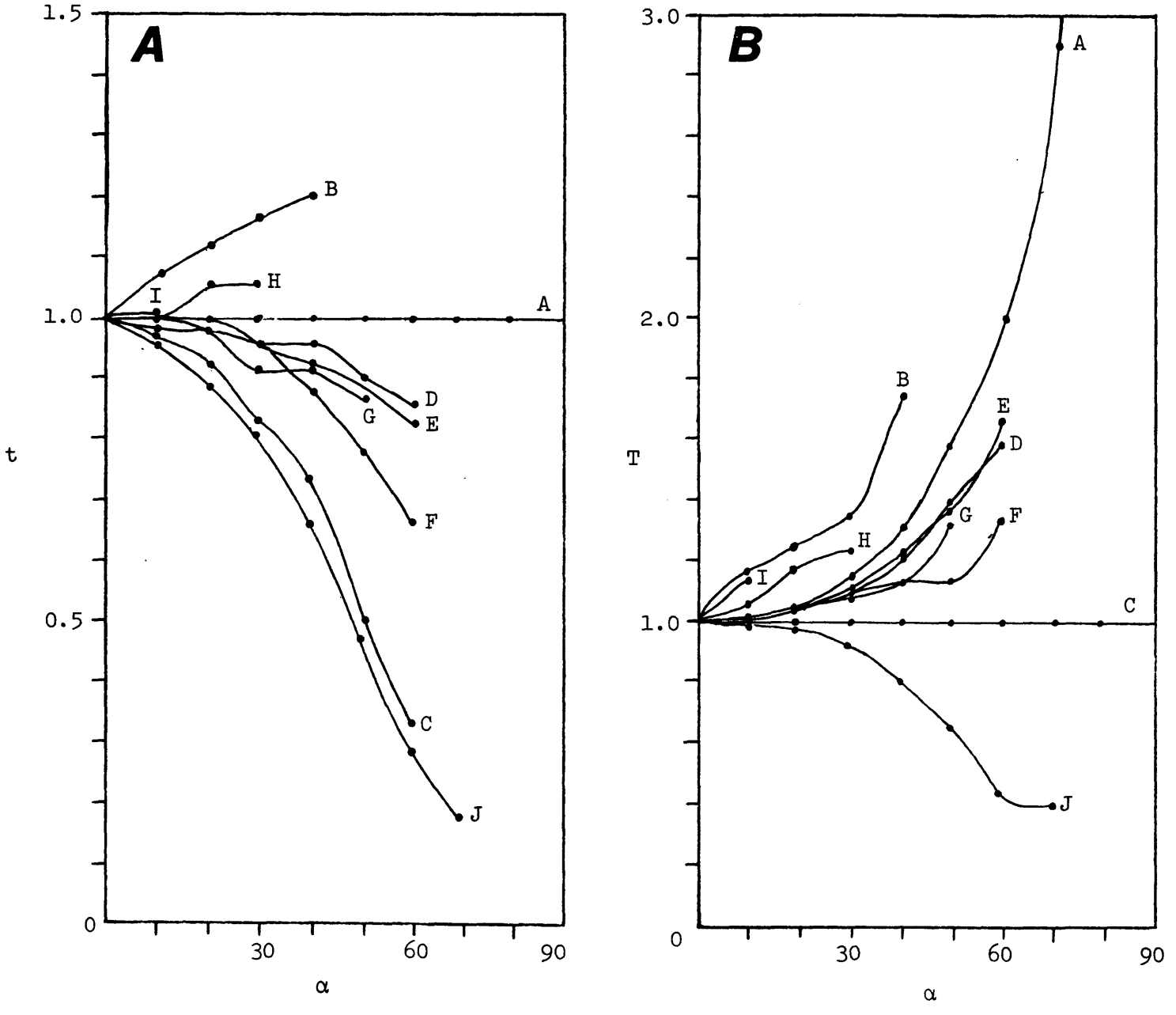

Fig. 6: T and t plots for layers from models of folds illustrated in Figure 5.

A, B: Idealised circular arc parallel fold.

C: Idealised similar fold.

D-I: Idealised paraboloidal parallel fold.

J: Idealised class 3 fold.

(1) Idealised pure circular-arc parallel fold (Fig. 5A).

The centres of arcs in a train of idealised circular-arc parallel folds all lie in a straight line. Billings (1954, p.58) showed that these folds cannot extend upwards or downwards in a fold stack beyond a certain thickness, which is governed by A and λ for the folds. Ramberg (1963) showed that in parallel folds there is a zone which consists of ideal parallel folds where the lengths of the individual layers remain constant. Outside this zone the layers have been affected by shortening and thickening. The thickness (D) of the central zone decreases if the amplitude increases for a constant wavelength, but increases for an increasing wavelength, provided the amplitude is kept constant.

If dip isogons are constructed on the model of idealised parallel folds drawn by Ramberg (1963, Fig. 10b) then fold layer A from the central zone is a class 1B fold of Ramsay (see Figs. 5A, 6). The layers outside the zone, represented by layer B, fall into class 1A. Hence the idealised parallel folds represented in Figure 5A consist of layers of both classes 1A and 1B, the dip isogons converging towards the inner arc of each layer.

(2) Idealised similar folds (Fig. 5B)

Ideal similar folds, as drawn by Ragan (1973, p.90), have dip isogons parallel to each other and also parallel to the axial surface of the fold stack, and hence are class 2 folds. T and t versus α curves (Fig. 6) are identical with the curves for theoretical class 2 folds presented by Ramsay (1967, p.366).

(3) Idealised paraboloidal parallel folds (Fig. 5C)

These parallel folds form a train in which the centres of curvature are non-linear (e.g. Billings 1954, Fig. 42B). The dip isogon patterns for several layers in the stack show systematic variations up or down the stack (Fig. 5C, Fig. 6). Fold layers D, E, F and G fall into class 1C, whereas layers H and I fall into class 1A. Between layers G and H the folds pass from class 1C, through class 1B which is not represented by a layer in this stack, to class 1A.

(4) Theoretical curves representing class 3 folds (Fig. 5D)

To provide a model of a stack of class 3 folds the paraboloidal parallel fold surfaces of Figure 5C were reversed in the stack to produce the folds in Figure 5D. Dip isogons and T and t versus $\measuredangle$ curves for layer J (Fig. 6) are typical of a class 3 fold.

In a fold stack it is possible to change from one fold class to another as the style of the layers change through the stack (see Fig. 5A and C). Hence it is possible to construct a model of a stack in which the layers change systematically from class 1A, through classes 1B and 1C to class 2 and return again to class 1A (Fig. 7B) or from class 1A through classes 1B, 1C and 2 to class 3 (Fig. 7A). Furthermore, class 1A folds exhibit strong differences in style in adjacent folded layers, class 1B only moderate differences and class 1C small differences. Class 2 folds have layers which maintain essentially the same style through the stack, while adjacent class 3 layers have different styles.

Apart from folds of class 2, each surface in a stack has a different interlimb angle. The folds illustrated in Figure 7 have a constant wavelength and hence A varies depending on C and θ. However while λ remains constant the ratio λ/L changes for each folded surface up and down the stack. The ratio λ/L for the folds in Figure 7A is greatest for the class 1A folds and some class 3 folds, is less for the class 1B and 1C folds and is at a minimum for class 2 folds. Hence, if θ for the inner arc is less than θ for the outer arc, there are class 1 folds. Conversely, for class 3 folds to occur, θ for the inner arc must be greater than θ of the outer arc.

Surfaces of class 2 in a fold stack will occupy only one position on the graphs of Figure 3 for each layer in a stack. This contrasts with other classes because for these folds in any stack, each surface will occupy a different position on the graphs. The position of surfaces 1 to 6 in Figure 7A changes progressively on a graph of λ/L against θ (Fig. 8A).

Dip isogons may also be used to measure the relative shortening or flattening of folded layers. If dip isogons are constructed for 10° intervals in a stack, then a measure of the spacing between isogons reflects the relative shortening and flattening that exists in a fold.

Maintenance of a constant length in the marker layers 1, 2 and 3 of Figure 7B can be achieved only if layers 1 and 3 are periodically kinked, or if there is a sharp increase in the dip of the limb relative to layer 2, because layer 2 is the longest and hence defines the original length of the

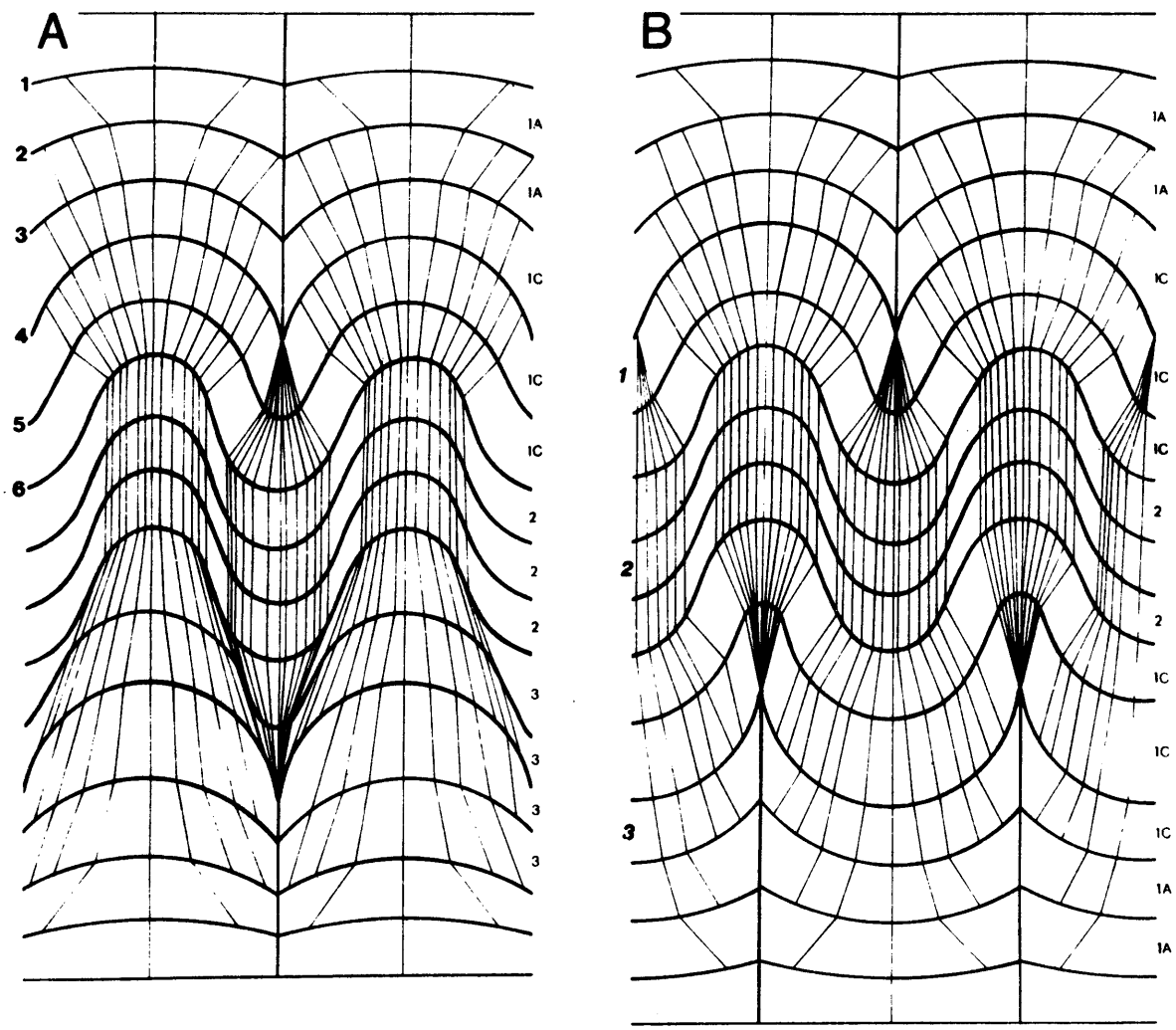

Fig. 7: Theoretical model of fold stacks where the layers change systematically through the fold classes of Ramsay (1967). See text p. 18 for full explanation.

layers before deformation. At least three alternative solutions to this problem can be proposed:

(1) parasitic folds may form on the limbs of the folds above and below the zone where class 2 folded layers are developing;

(2) a sudden sharp increase may occur in the dip of the limb of a layer relative to the dip of the class 2 layer; and

(3) if buckling is occurring then eventually a new s-surface may be produced along which slip may occur and gleitbretter structures may form in an attempt to maintain layers 1 and 3 at the same length as layer 2. If this happens, then, geometrically speaking, buckle folds grade into gleitbretter slip folds and a new s-surface is produced.

INFLECTION SURFACES

A useful element for describing one aspect of the geometry of folds is the locus of the lines of inflection of the limbs in a fold stack. This has been termed the inflection surface by Verhoogen *et al.* (1970, p.153) who also took the inflection line as the limit of a single fold in the surface.

Most folded surfaces have a variable curvature in the profile plane. $\frac{dy}{dx}$ is a measure of the gradient of the curve and $\frac{d^2y}{dx^2}$ is the rate of change of the gradient of the curve. The crest (Point B in Fig. 8B) has $\frac{dy}{dx} = 0$ and is a maximum turning point whereas the trough (Point A) is a minimum turning point. A point of inflection (Point C) is defined as the point where $\frac{d^2y}{dx^2} = 0$ and $\frac{dy}{dx}$ does not change sign on either side of the point. For some folds the limbs are straight and hence the gradient does not change over this distance. Consequently $\frac{d^2y}{dx^2} = 0$ for the entire length of the limb. Ramsay (1967, p.347) defines the inflection point on such a limb as the midpoint of the straight portion, but that device is not rigorous because a single point of inflection does not exist. In this thesis two "change points" for each straight limb are used and are defined as points where $\frac{d^2y}{dx^2} = 0$, and on the side of the point towards the hinge $\frac{d^2y}{dx^2}$ is changing, and on the other side away from the hinge $\frac{d^2y}{dx^2} = 0$.

For folds with straight limbs between the hinge zones, a zone of constant curvature exists, (here defined as Z), the thickness of which can be related to the style of folds. Z is related to A such that $0 \leqslant Z \leqslant 2A$. As the thickness of Z decreases the chord length (c) increases according to the following formula for symmetrical folds:

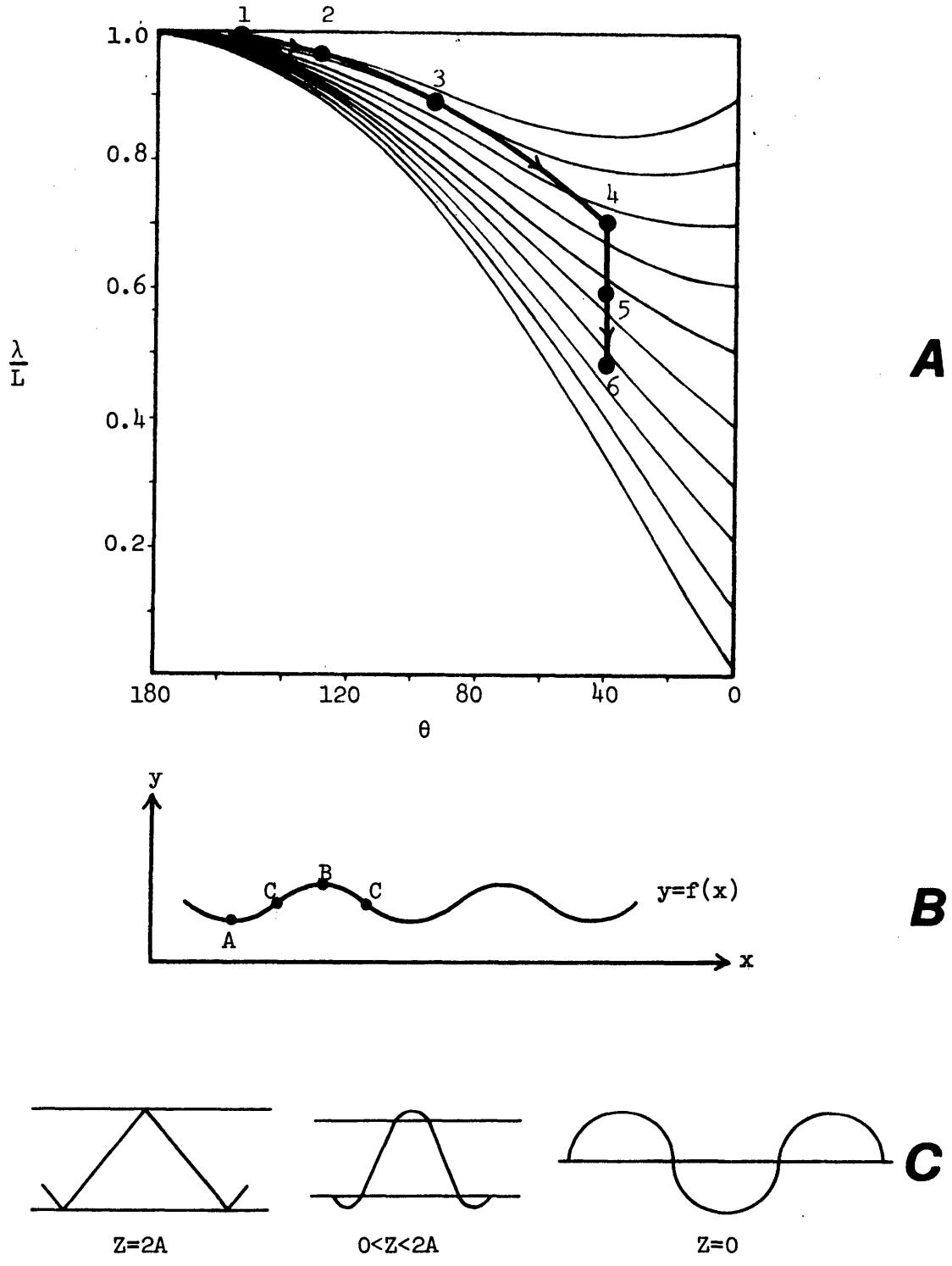

Fig. 8 A: Migration path of surfaces 1-6 of fold stack illustrated in Figure 7A.

B: Crest, trough and points of inflection for the trace of a single folded surface in the profile plane.

C: Schematic illustration of the three general cases for $0 \leq Z \leq 2A$ for the zone of constant curvature.

$Z = \frac{1}{2 \tan (\frac{\theta}{2})} \cdot (\frac{\lambda}{2} - c)$. Substituting $0 \leqslant Z \leqslant 2A$ into this equation, three general cases occur:

(1) $Z = 2A$. This is the case for angular folds because $C = 0$ (Fig. 8C).

(2) $0 < Z < 2A$. This is the general case for folds with rounded hinges and straight limbs (see Fig. 8C).

(3) $Z = 0$. The change points are coincident with the inflection point and the surface is a pure circular-arc parallel folded surface (see Fig. 8C). Here $\theta = 0$ and $\lambda = 2C$.

Hence, in the profile plane a folded surface has either change or inflection points. These points represent lines of inflection or change lines from adjacent surfaces in a stack, and the locus of the lines in a stack is a fold stack inflection surface (SIS) or fold stack change surface. If inflection or change lines in a fold train are connected they produce a fold train inflection surface (TIS) or a fold train change surface. Using as examples the folds illustrated previously (Fig. 5), the inflection surfaces for trains and stacks are illustrated in Figure 9. A useful measure is the angle between SIS and axial surface trace (AS) in the profile plane (ϕ = SIS < AS). ϕ ranges between 0° and 90°.

(1) $\phi = 0°$. Here SIS $/\!/$ AS and two cases occur within this category:

(a) Idealised similar folds (Fig. 9A). The TIS for an idealised similar fold constitute a series of equidimensionally spaced parallel lines perpendicular to AS. SIS also constitute a series of equidimensionally spaced parallel lines. However the SIS are parallel to the AS and are midway between them. The spacing between SIS and TIS differs, depending on λ, A and the thickness of individual layers. SIS is normal to TIS and if these conditions are met, then class 2 folds occur.

(b) Angular folds (Fig. 9B). Again we have $\phi = 0$ and SIS$\perp$TIS. However, the main difference from the idealised similar folds is that AS and SIS are coincident. For a single folded surface with sharp hinges and two TIS separated by a distance Z, then the two TIS are coincident with the enveloping surfaces which define the outer limits of the fold.

(2) $\phi = 90°$, SIS$\perp$AS. These folds are idealised circular-arc parallel folds (Fig. 9C). The surfaces in the central zone have not suffered the effects of shortening and thickening, and hence all SIS are coincident with each other, and perpendicular to AS. Also within this zone the TIS are coincident with the SIS. Consequently class 1B folds have all SIS coincident with all TIS and perpendicular

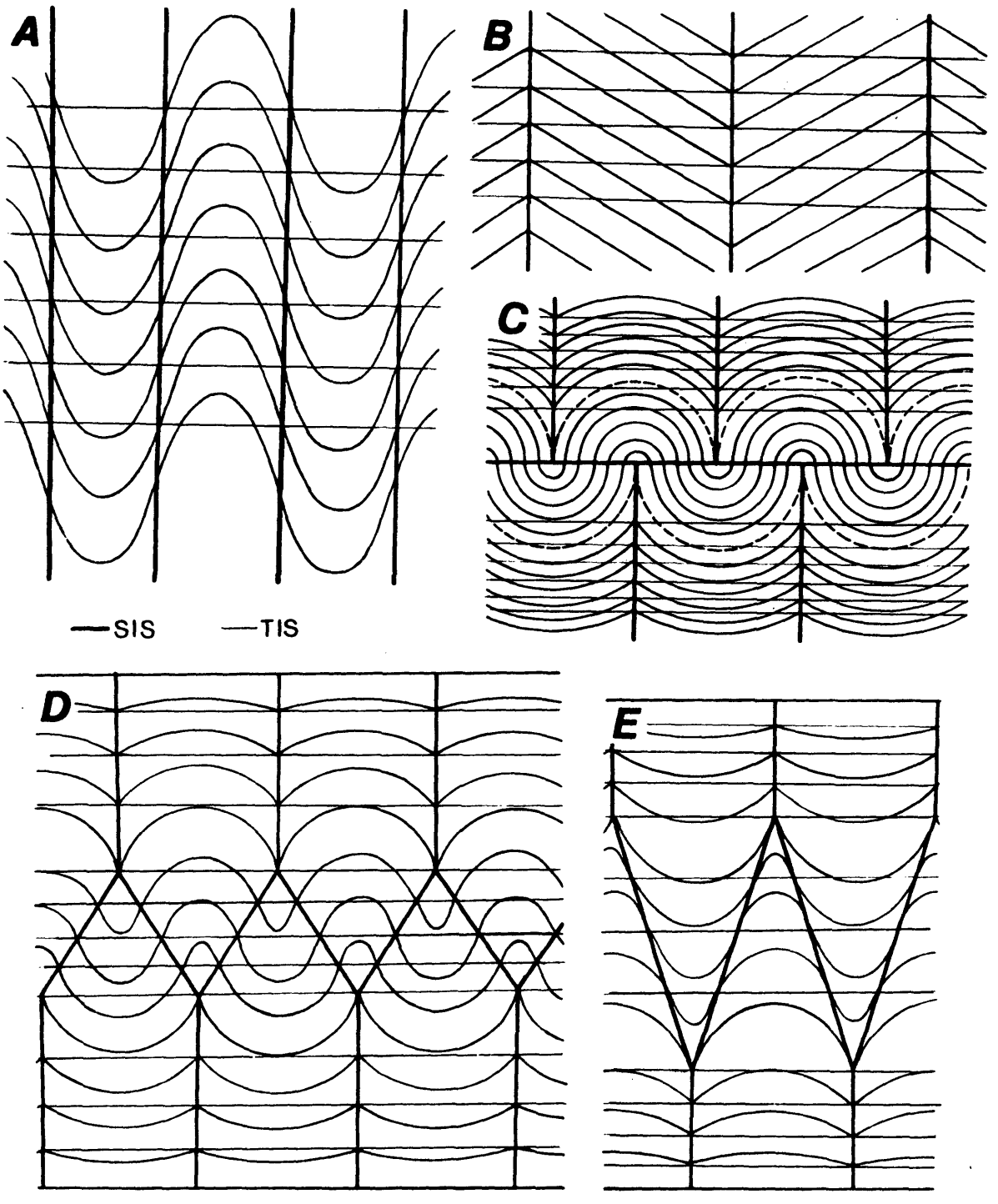

Fig. 9: Fold stack inflection surfaces and fold train inflection surfaces for theoretical fold models. A - idealised similar fold, B - angular fold, C - idealised pure circular-arc parallel fold, D - idealised paraboloidal parallel fold, E - theoretical model of class 3 fold.

to AS. However, on moving out of the central zone into the layers with class 1A style, then SIS becomes parallel to AS, and coincident with it in places, and the TIS become equidimensionally spaced perpendicular to AS.

(3) $0° < \phi < 90°$. This condition occurs with some fold surfaces of class 1C and class 3 (Fig. 9D and E). The centres of the folds have become non-linear. Here TIS remains normal to AS but SIS defines a zigzag locus from one centre to the next. In Figure 9D $\phi = 30°$ and in Figure 9E $\phi = 18°$.

Johnson and Ellen (1974, Fig. 11) illustrate lines of discontinuity in ideal "concentric" folds. Their line of discontinuity is the same element as the SIS for paraboloidal parallel folds illustrated here (Fig. 9D). This indicates Johnson and Ellen's ideal "concentric" fold is not a pure circular arc parallel fold but is a paraboloidal parallel fold.

4. ATTITUDES OF FOLDS, AND RELATIONSHIPS OF THE MARKER HORIZON TO THE AXIAL SURFACE

The attitudes of folds may be described by reference to the orientation of the axial surfaces and fold axes. Fleuty (1964 pp. 481-488) proposed a scheme whereby the dips of axial surfaces and plunge of fold axes are subdivided into numerical sectors given appropriate names. His nomenclature is followed here.

The general problem of variably oriented fold axes was discussed earlier (p.5) along with solutions to the problem that have been proposed in the literature. Another theoretical solution is proposed here, and an attempt to apply it to rocks from the Coffs Harbour Block will be made in Chapter 2.

If one supposes that a folded surface (SF) was originally horizontal, then as the intensity of folding increases, the dips of the folded surface must become steeper, until finally the bedding could become vertical and isoclinal folds could be formed. It is convenient for further analysis to assume that the axial surface (SG) maintains a constant orientation during deformation. variable factors, upon which the following discussion rely, are then:

(i) dip of SF, plus dip direction, (one limb only of a fold being considered);

(ii) angle between the strike of SF and strike of SG; and

(iii) plunge and trend of the fold axis (FA).

A special case occurs when the strike of SF is parallel to the strike of SG. As the dip of SF changes, there is then no change in the plunge of FA, which always remains horizontal. In another special case, when SG is horizontal the plunge of FA is again always zero.

The fold axis is determined by the intersection of SF and SG (see Fig. 10A). FA is represented by the line OA (Fig 10B) and its orientation is represented by a plunge (angle ϕ, from horizontal) and trend (angle θ, from North or y, measured in the horizontal plane). In this case OA represents the intersection of SF and SG. In the general case OA represents any B lineation, including those generated by the intersection of two planes.

Using Fig. 10B,

plunge = $\angle$POA = ϕ, trend = $\angle$YOP = θ

Let distance OY = y, YP = x, PA = z

Let distance OP = p, and OA = unity

In ΔPOA, $\sin \phi = z$

$\cos \phi = p$

In ΔYOP, $\sin \theta = \frac{x}{p}$

$\cos \theta = \frac{y}{p}$

$x = \cos \phi . \sin \theta$

$y = \cos \phi . \cos \theta$

$z = \sin \phi$

Hence x, y, z are the direction cosines for the vector OA. Now using direction cosines:

(1) Plane SF. Using the normal to the plane, trend = θ_1, plunge = ϕ_1, direction cosines are: $a_1 = \cos \phi_1 . \sin \theta_1$

$b_1 = \cos \phi_1 . \cos \theta_1$

$c_1 = \sin \phi_1$

(2) Plane SG. Using the normal to the plane, trend = θ_2, plunge = ϕ_2, direction cosines are: $a_2 = \cos \phi_2 . \sin \theta_2$

$b_2 = \cos \phi_2 . \cos \theta_2$

$c_2 = \sin \phi_2$

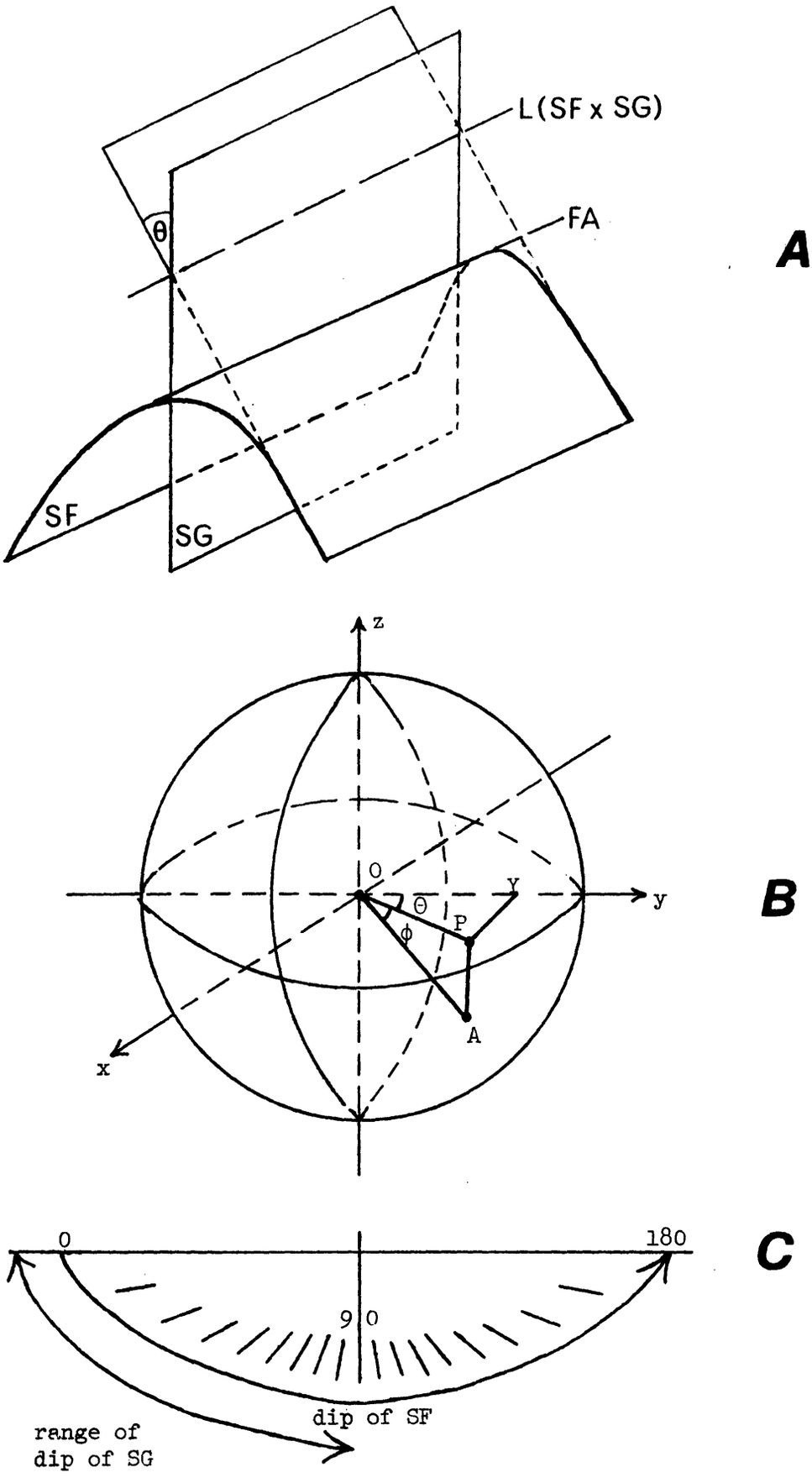

Fig. 10: Diagrams illustrating use of nomenclature in determining relationships of the marker horizon to the axial surface. For full explanation see text pp. 21-25.

Hence by solving the simultaneous equations:

$$a_1x + b_1y + c_1z = 0 \qquad \text{---------- (1)}$$

$$a_2x + b_2y + c_2z = 0 \qquad \text{---------- (2)}$$

$$x^2 + y^2 + z^2 = 1 \qquad \text{---------- (3)}$$

Using equations (1) and (2),

$$\frac{x}{b_1c_2 - c_1b_2} = \frac{-y}{a_1c_2 - a_2c_1} = \frac{z}{a_1b_2 - a_2b_1} = k$$

$$\therefore \quad \left.\begin{aligned} x &= k(b_1c_2 - c_1b_2) \\ y &= k(a_2c_1 - a_1c_2) \\ z &= k(a_1b_2 - a_2b_1) \end{aligned}\right\} \qquad \text{---------- (4)}$$

Substitute (4) into (3)

$$k^2(b_1c_2 - c_1b_2)^2 + k^2(a_2c_1 - a_1c_2)^2 + k^2(a_1b_2 - a_2b_1)^2 = 1$$

$$k^2 = \frac{1}{(b_1c_2 - c_1b_2)^2 + (a_2c_1 - a_1c_2)^2 + (a_1b_2 - a_2b_1)^2}$$

$$k = \sqrt{\frac{1}{(EXP)}} \qquad \text{---------- (5)}$$

By substituting (5) into (4) the values of x, y, and z are found. As x, y, and z are the direction cosines for the resultant vector OA, the plunge (ϕ_3) and trend (θ_3) of OA are derived.

By substitution of different values for the plunge and trend of the normals to SF and SG, it is possible to calculate a series of values showing the systematic variation of the plunge of the intersection of the two planes. The results presented in the following discussion have been calculated by program SAVSB (see Appendix II). An alternative very tedious method is to plot intersections of SF and SG on a stereographic projection to obtain the plunge and trend of the resulting lineation.

Using the results from program SAVSB, it is possible to construct a series of graphs for different fixed dips of SG and changing dips of SF. If 10° intervals are used for SG then nine graphs representing the dips of SG from 10° to 90° could be presented, but for brevity only three examples are

actually presented using values for the dip of SG of 90°, 80° and 30° (Fig. 11). On each graph a set of curves shows the changes in plunge of a lineation produced by the intersection of an SF of variable dip and fixed strike with an SG of fixed orientation. The dip of SF on each graph ranges from 0° to 90° in the direction of the dip of SG, and then from 90° to 0° in the opposite direction to the dip of SG (see Fig. 10C). This is represented by the figures 0° to 180° on Figure 11.

From Figure 11 it is evident that the plunge of FA is controlled by the dips of SF and SG if the two surfaces have different strikes, and SF ranges from horizontal towards vertical. Only very small differences in strike however produce effects: even a difference of only 1° causes remarkable changes in the plunge of FA when the dip of SF is close to the dip of SG.

In the general case, if the marker horizon (SF) is horizontal, and a vertical SG develops then the resultant FA is horizontal. If SF is slowly deformed the limbs of the developing fold become steeper. Keeping SF with a constant strike, it can be seen that the plunge of the FA depend on the dip of SF. Now if the strike of SF is constantly at an angle of 10° to the strike of SG then as deformation proceeds, the dip of SF becomes steeper and the plunge of FA changes from 0° when SF is horizontal to 90° when SF is vertical. Hence it is possible, using the geometric arrangement described above, to have the plunge of FA changing progressively from 0° to 90° even though SG retains a constant orientation. The only constraint is that the strikes of SF and SG must not be parallel.

Figure 12 shows graphically the migration of lineations caused by a progressive steepening of a form surface. In the model outlined previously the orientation of SG remains constant. However, on the stereographic projections of Figure 12 the cyclographic traces of SG are shown in different positions for each change in the angle between the strikes of SF and SG. This is done to avoid overprinting of the movement paths of the lineations.

Sander (1970) briefly outlined the geometry of the intersections of meridians and parallels, and then elaborated to show the changes in the position of B if the strike of the s-surface or the axial trend altered. *"If we vary the dip of s from 0° to 90°, the axial plunge with constant axial trend changes at an increasing rate"* (Sander 1970, p.167). He was concerned with showing that errors in the measurement of s-surfaces caused large errors in the determination of the plunge of FA, particularly if only a small divergence occurred between the strikes of SF and SG. Apparently he did not realise that his analysis could also solve the problem of changes in plunge

that are real (and not artefacts of errors in attitude measurements). The black dots in Figure 63 of Sander (1970) show the same pattern as in Figure 12A and his figure is a specific example of the model outlined above (SG vertical; variable dip and strike of SF). The diagram can be used also to keep SF with constant strike and variable dip, and SG with constant dip but variable strike.

This model could be extended to determine the movement paths for lineations where the orientation of SG remains constant while both the dip and strike of SF are changing, (so that the angle between the strikes of SF and SG is changing). Using data from SAVSB, Figure 13A represents a constant SG intersected by an SF which is rotating from horizontal to: dip 1°, strike difference 89°, ... dip 10°, strike difference 80°, ... dip 70°, strike difference 20°, ... dip vertical, strike difference zero; with all dips of SF in the same direction as the dip of SG. The movement paths for the lineation trace out complex curves for changing dips of SG with a constant strike direction (Fig. 13B). Hence, it would be possible using the results of SAVSB, to construct the structural movement path for a lineation produced by the intersection of SF and SG if both were changing in orientation simultaneously.

5. FORM AND DESCRIPTION OF CLEAVAGE

The main problem with the cleavage observed in the Coffs Harbour region is to explain the development of a cleavage such as illustrated in Plate 3. As indicated previously when outlining the problem (p. 6), this cleavage has features characteristic of both slaty and fracture cleavages, in that it appears to grade from a "fracture" cleavage to a slaty cleavage within one lithological type.

An hypothesis of origin starts with the assumption that the initial marker layer (SF) is planar and is being gradually deformed. Because the rock mass is not homogeneous throughout it is not perfectly viscous and therefore tends not to flow but to move along discrete planes. These planes are parallel to the axial surface of the fold and occur as an early cleavage (SG_1 in Fig. 14). The intersection of SF and SG_1 defines a lineation parallel to FA_1.

As the marker layer (SF) is deformed further, the original cleavage (SG_1) is rotated along with the marker layer. At a later stage a second cleavage (SG_2) develops parallel to AS and cuts the earlier cleavage forming a

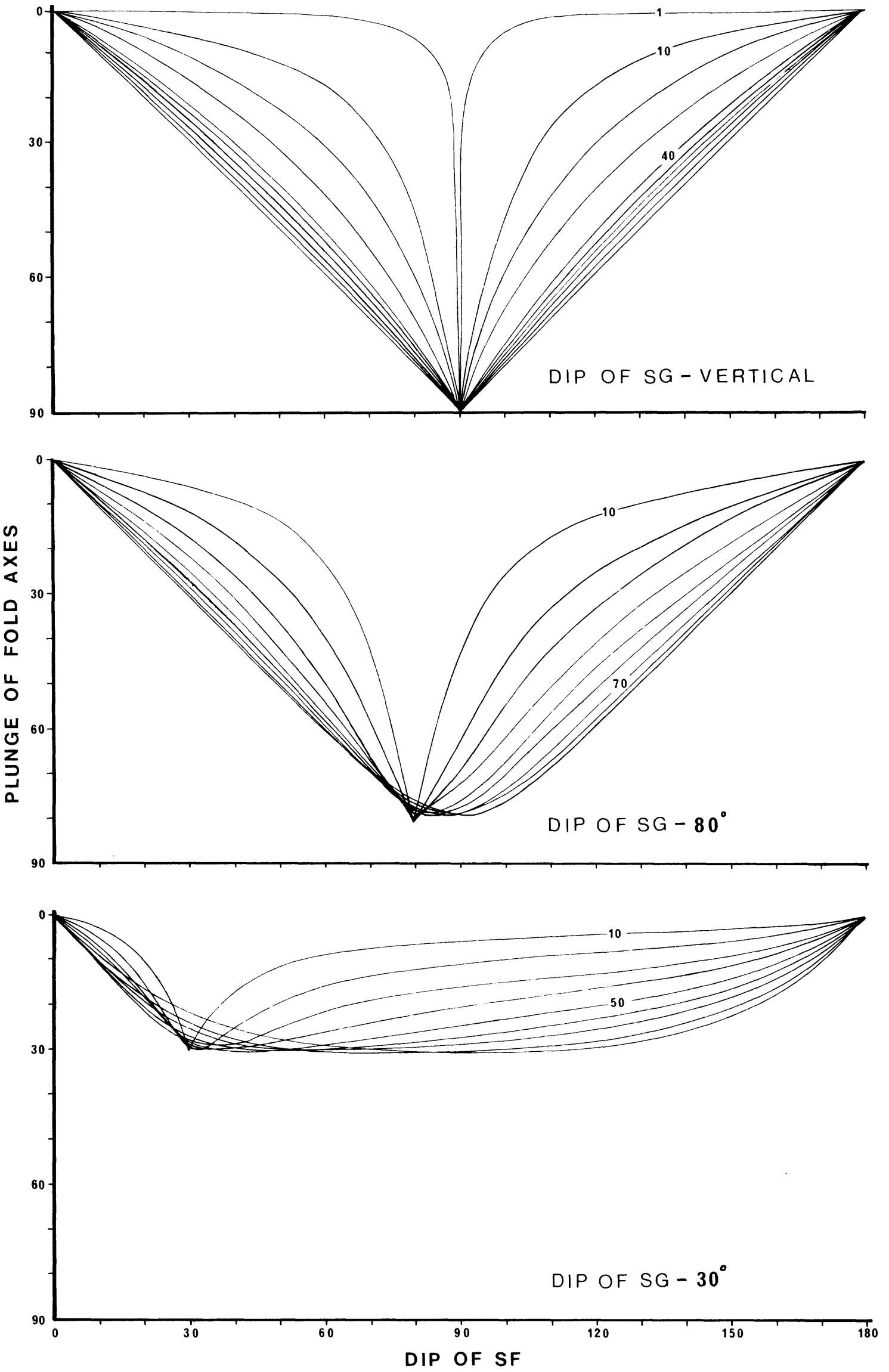

Fig. 11: Changes in plunge of an FA produced by the intersection of an SF of variable dip and fixed strike with an SG of fixed orientation.

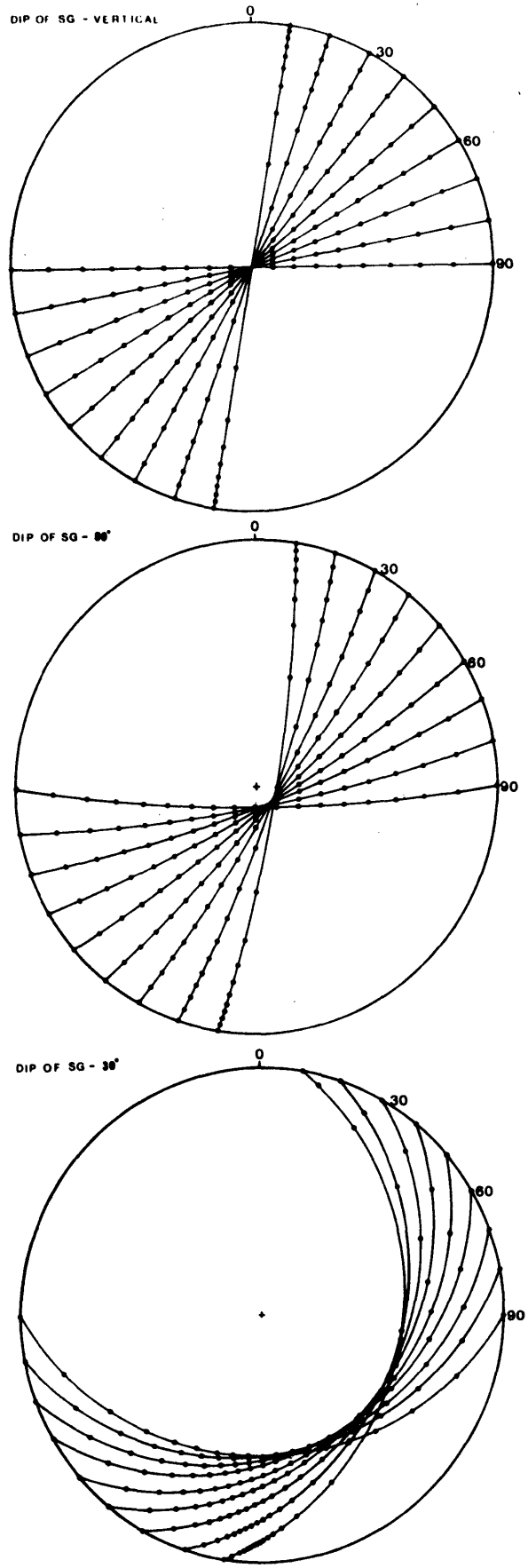

Fig. 12: Structural movement paths of lineations for intersection of SF and SG. For full explanation see p. 24.

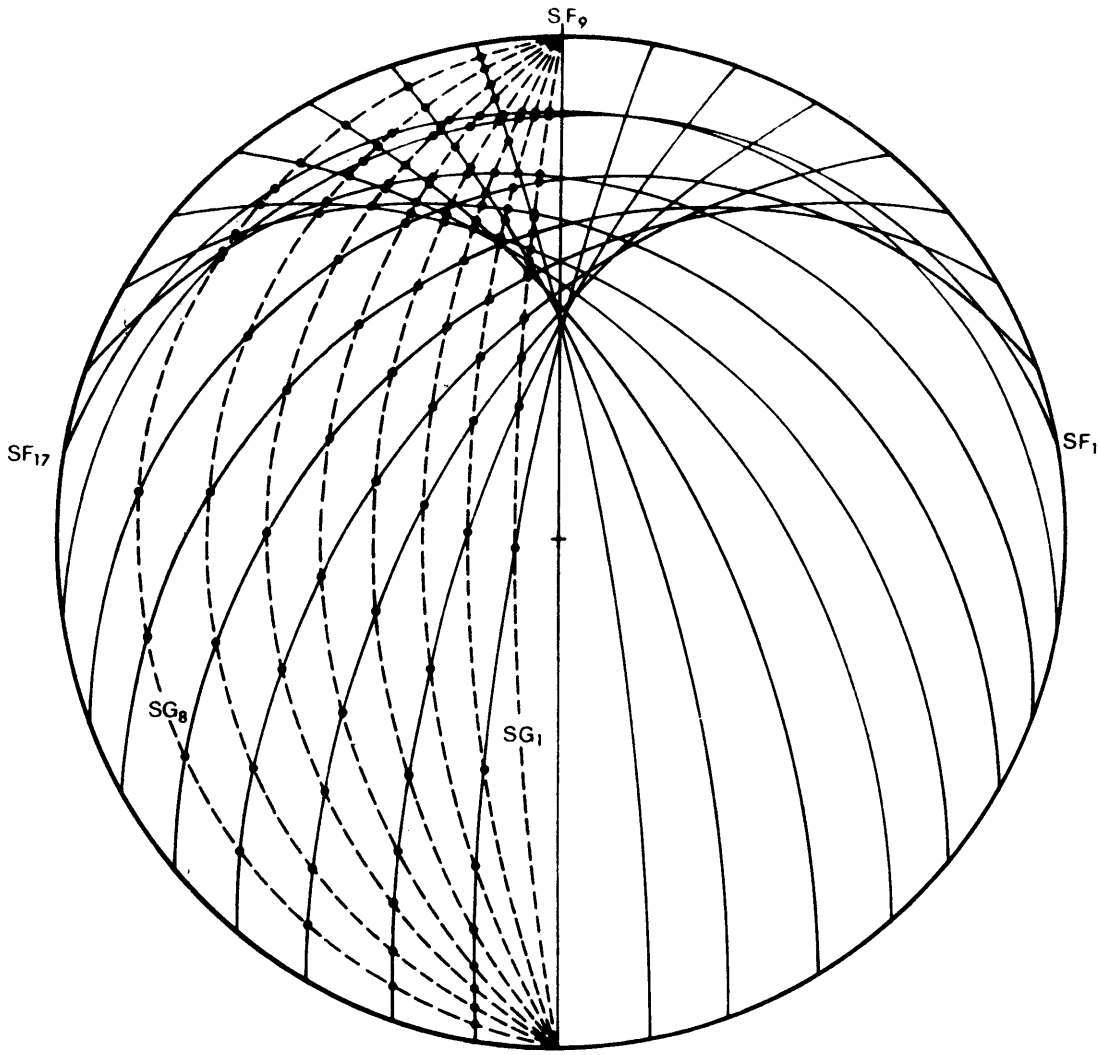

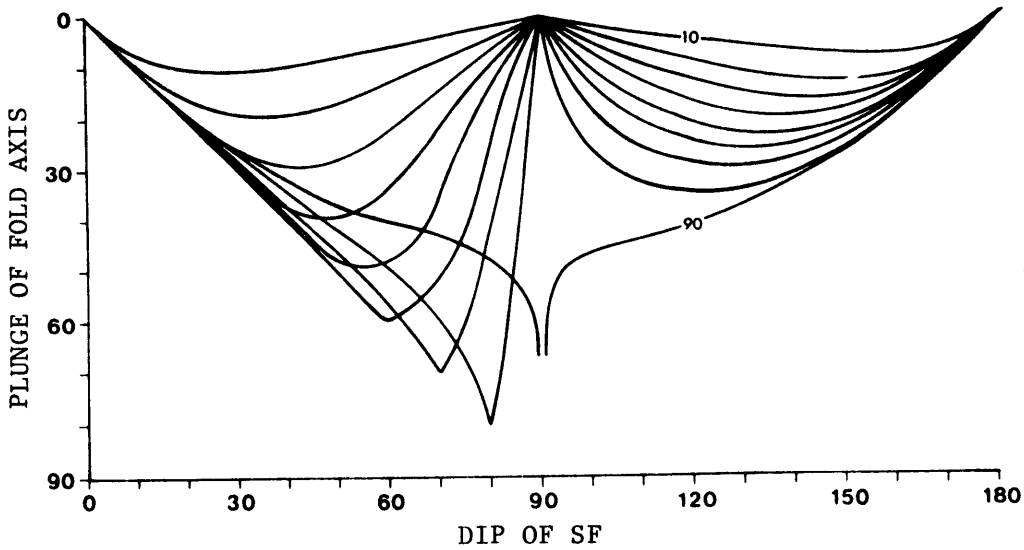

Fig. 13: Stereographic projection and change in plunge of the fold axis for a situation with a constant SG being intersected by an SF for which both the strike and dip are changing.

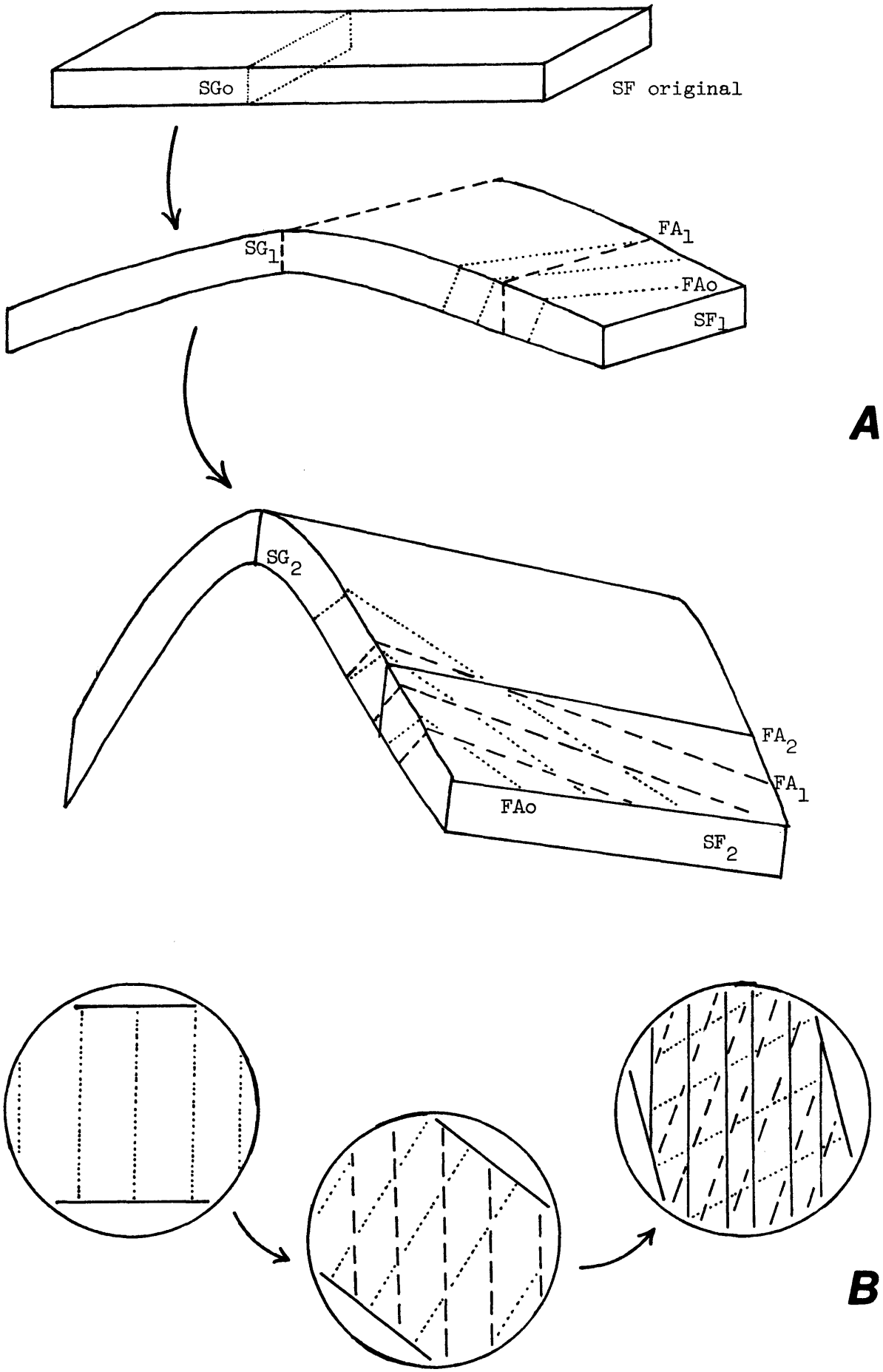

Fig. 14 A: Rhombic pattern of intersections developing due to truncation of an early cleavage by a later cleavage.

B: Enlargement of a small part of the limb for the three stages illustrated in Fig. A.

rhombic intersection pattern (Fig. 14). If the strike of SF remains constant the lineations produced (FA_1, FA_2) will be parallel but if the strike of SF_2 is different from that of SF_1 then FA_1 and FA_2 will not be parallel and will intersect to form a rhombic pattern on the surface of the marker layer. A rhombic pattern is observed in the profile plane of the layer (Fig. 14).

The rhombic pattern can be analysed mathematically using the following parameters (see Fig. 15A):

s = spacing between two adjacent SG_2 cleavage planes,
θ = angle between SG_1 and SG_2,
1 = length of SG_1 truncated by two adjacent SG_2.

From the right-angle triangle,

$$\sin \theta = \frac{s}{1}$$

$$\therefore 1 = \frac{s}{\sin \theta}$$

Figure 15B illustrates a series of curves using the above formula. Each curve is for a constant spacing value (s = 0.5 to 10.0) and a variable angle between the two cleavage planes ($0° \leqslant \theta \leqslant \pm 90°$). From Figure 15B the following points arise:

i. When $\theta = 0°$, SG_1 is parallel to SG_2 and $1 = \infty$. In practice the length 1 is controlled by the longest observable cleavage plane.

ii. When $\theta = 90°$, $s = 1$ and the minimum length of SG_1 is defined as the spacing between adjacent SG_2 planes.

iii. The illustrated curves represent the situation for both limbs of a fold. In practice only one side of the y-axis should be represented for any one situation (except in the hinge region) and the curve represents differing values of 1 as SG_1 rotates from parallelism with SG_2 to being normal to SG_2.

Predictions about cleavage from the theoretical model

1. In the hinge region of a fold the successive cleavage planes remain parallel at all stages.

2. The most distinct and continuous cleavage planes should be the last to form, as they truncate earlier surfaces. The orientations of SG should diverge from the stronger to the weaker either dextrally or sinistrally

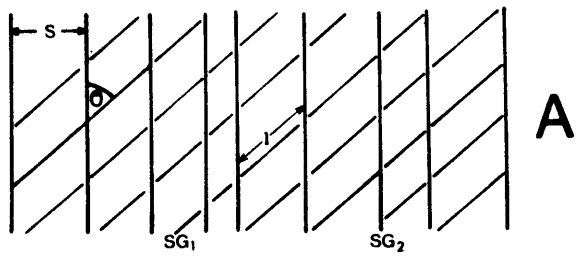

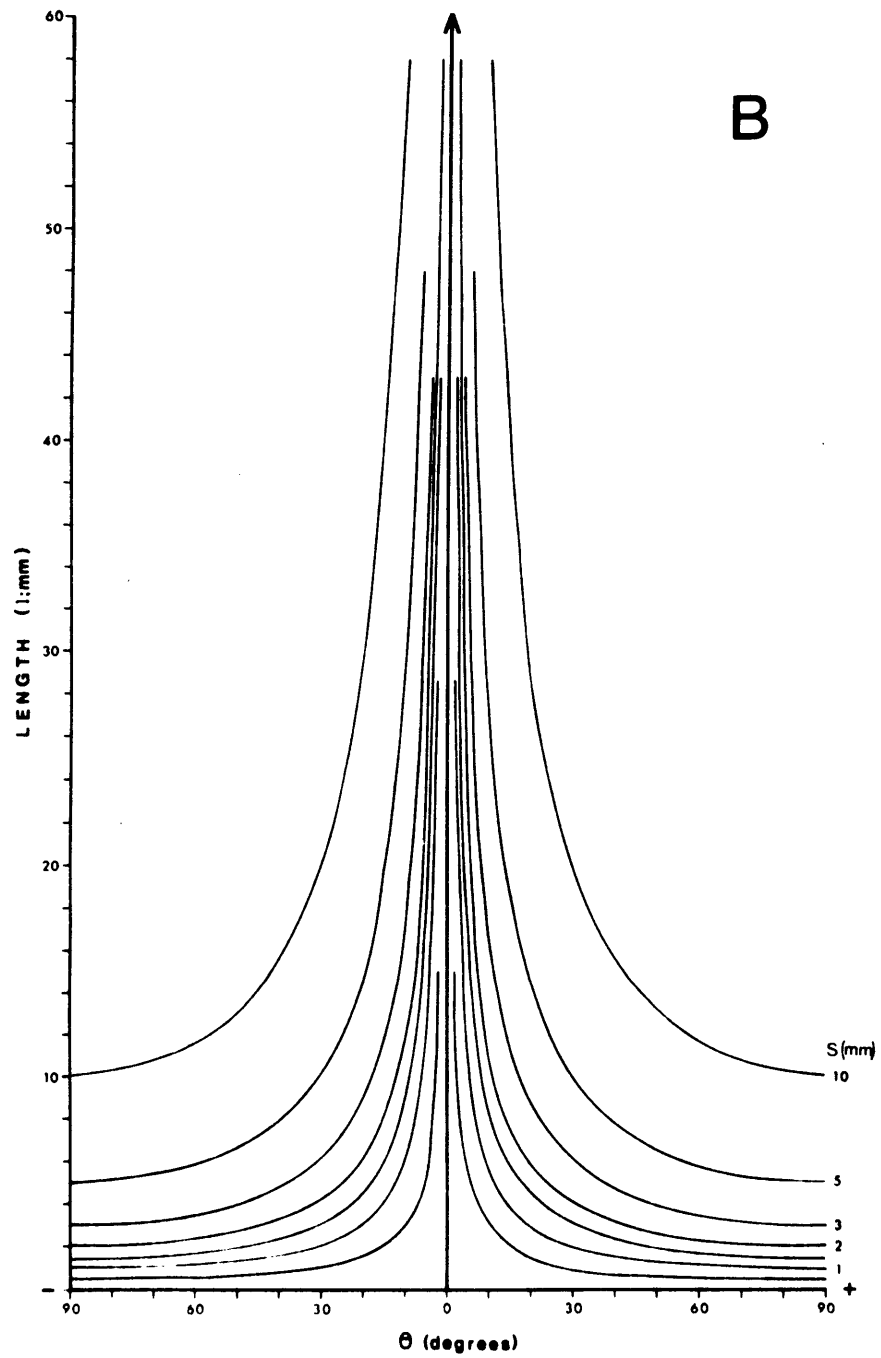

Fig. 15 A: Parameters used for theoretical analysis of cleavage.

B: Theoretical curves for cleavage patterns. For full explanation see text pp. 25-27.

but not in both directions. The sense of divergence should allow an observer to determine on which limb of a fold an area or specimen is located.

3. There should be a good correlation between the lengths and directions of different cleavage surfaces, the longest SG trace being parallel to the present axial surface and the shorter traces being divergent from it.

4. If several periods of cleavage development have occurred then each later cleavage surface should truncate or partly obliterate the earlier cleavage surfaces. The earliest cleavage will be the most severely affected because it lies at the greatest angle to the last-formed SG. Cloos (1947, p.878) has shown that as deformation proceeds in a folded layer, cleavage begins to appear only after a shortening deformation of thirty percent has occurred. After the material has been deformed fifty percent, a faint parallelism of particles appears in the cleavage direction. Hence cleavage will not develop in the early stages of folding and therefore early cleavage planes should not occur at large angles to the later cleavages.

5. The development of cleavage may be a continuous process where SG_1 is formed, rotated and overprinted by SG_2, which is overprinted by SG_3 and so on. If the deformation is not severe the earlier cleavage may not be destroyed, resulting in the rhombic pattern of a fracture cleavage. For a severe deformation a later closely-spaced cleavage might completely obliterate an earlier cleavage, resulting in the development of a slaty cleavage.

The above idea contrasts with the conclusion of Powell (1974) that slaty cleavage associated with folded Precambrian slates and quartzites in northwest Tasmania was formed in a short time interval during a period of protracted folding.

The relationships between SF, SG and the lineations produced by the intersections of the various surfaces are now shown graphically for two cases, using data from only one limb of a fold (Figs. 16 and 17).

Notation used in text and figures

1. SF - marker layer. SFo is the original marker horizon being rotated at 10° intervals, through successive positions labelled as SF_1 to SF_9.

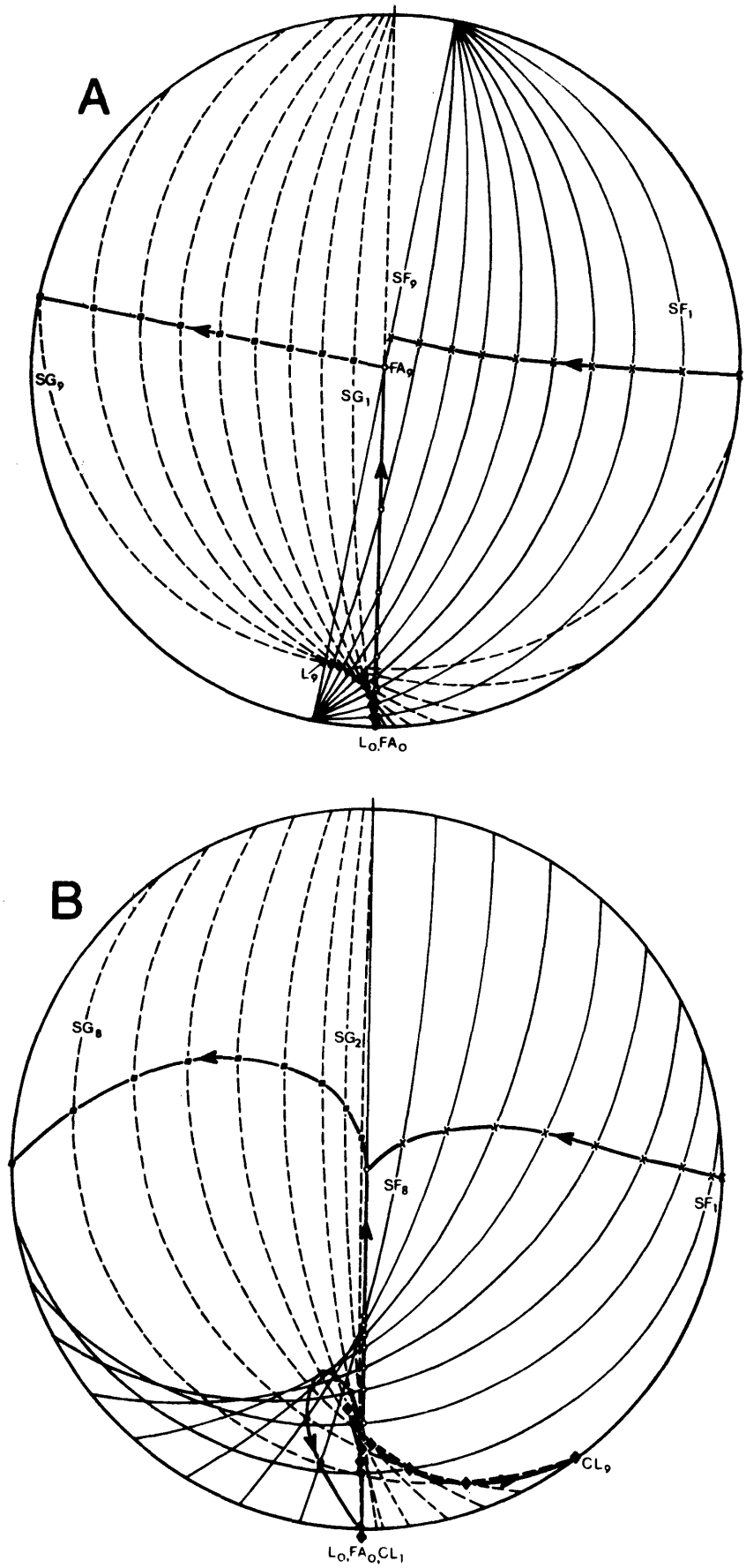

Fig. 16: Graphic relationships between SF, SG and the lineations produced by the intersections of the various surfaces. — SF, --- SG, × pole to SG, ■ pole to SF, ○ FA, • L, ◆ CL. For full explanation see text pp. 27-29.

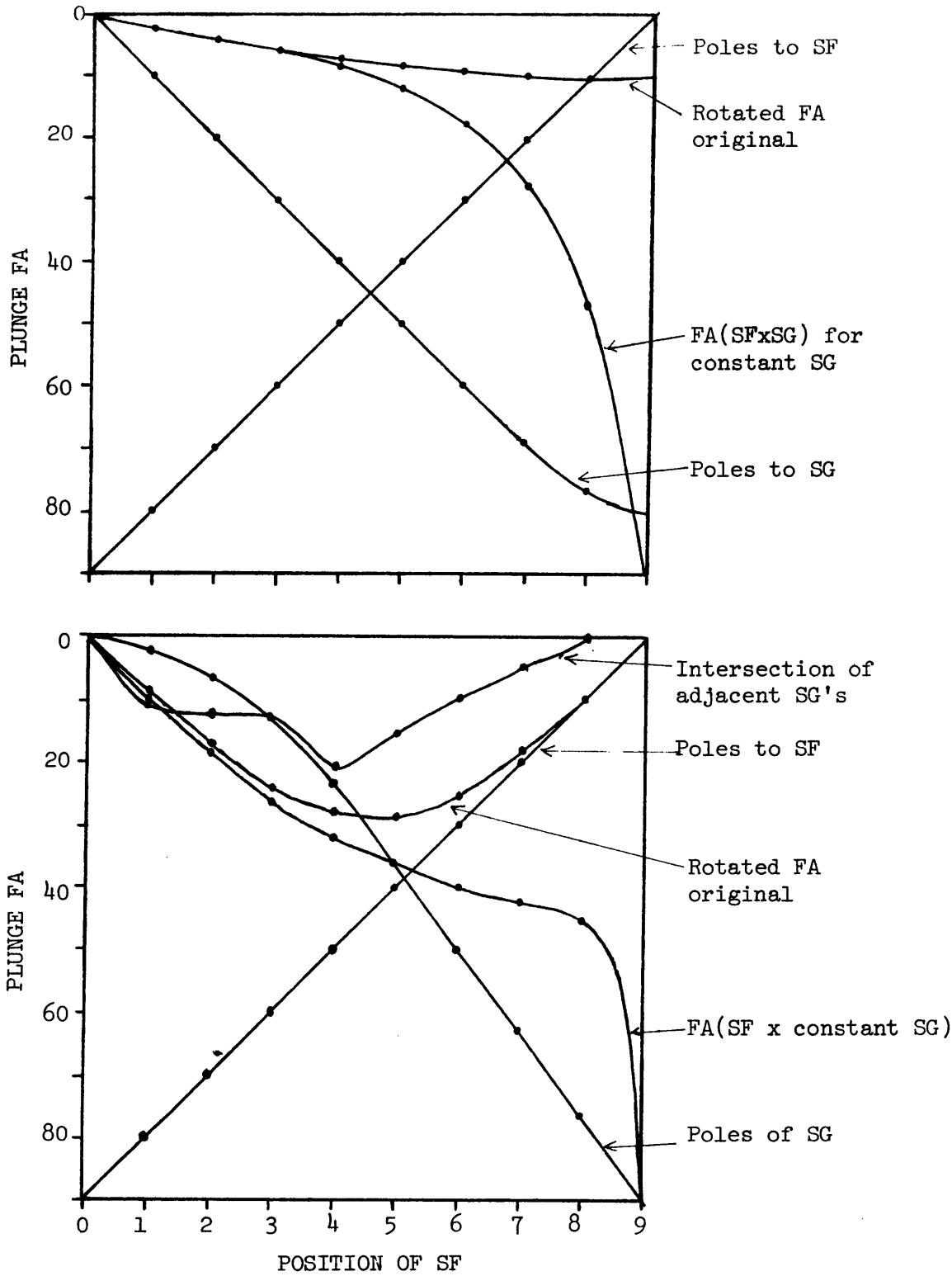

Fig. 17: Migration paths of lineations produced by intersections of the various surfaces illustrated in Figure 16. For full explanation see text pp. 26-29.

2. SG - SGo is position of axial surface and original cleavage plane. As SFo is rotated to SF_1 the original cleavage is rotated to position SG_1 and a new (second) cleavage forms at SGo. As SF_1 is rotated to SF_2 the original cleavage is now rotated to position SG_2 and the second cleavage rotates to SG_1. A new (third) cleavage forms at SGo ... and so on to SG_9.

3. FA - Fold axis produced by the intersection of a constant AS (SGo) with the marker layer SF. FAo to FA_9 represent the positions of the fold axis for successive rotations of SFo to SF_9.

4. L - Lo to L_9 are positions of the lineation produced by the intersection of SFo and SGo and subsequently rotated in the cleavage plane from SGo to SG_9 as SF is rotated from SF_1 to SF_9.

5. CL - CL_1 to CL_9 are positions of lineations produced by the intersection of adjacent cleavages, e.g. CL_8 is the position of the lineation resulting from the intersection of SG_7 and SG_8.

CASE A: This case has SF which maintains a constant strike orientation but a variable dip from 0° to 90° (Fig. 16A). The angle between the strike of SF and the strike of AS remains constant at 10°. The AS maintains a constant strike and vertical dip.

As the dip of SF rotates about its strike from the horizontal towards the vertical, the fold axes (FAo to FA_9) become increasingly steeper with increasing dip of SF. For a cleavage formed parallel to AS (SGo) the subsequent rotations of SF will rotate SGo through successive positions labelled SG_1 to SG_9 in Figure 16A. The structural movement paths, traced out by the rotation for the poles to SF and SG are indicated in Figure 16A and the variation in plunges for the lineations and poles are graphed in Figure 17A. The rotation of the original lineation Lo (SFo x SGo) through positions L1 to L9 traces out a movement path which changes only 10° both in plunge and trend during the entire rotation. Hence while the plunge of the fold axis is changing rapidly, the originally formed lineation (once parallel to FAo) is being rotated only a relatively small amount.

CASE B: This case has a constant vertical AS (SGo) while SF has changing strikes and dips. The angle between the strike of SFo and SGo is originally 90° and SF is horizontal. The angle becomes less as SF rotates and steepens and is finally zero when SF is vertical and parallel to SGo (Fig. 16B). FA_6 to FA_9 steepens rapidly at first then steepens less rapidly as the higher

dips of SF (50° to 80°) are approached. Lo to L9 trace out a structural movement path returning to its origin so that Lo and L9 are coincidental. Hence lineations L6 to L9 have similar trends to Lo to L5 and may have obliterated the earlier lineations leaving only one dominant orientation for L.

CLo to CL9 trace out an unusual pattern. The plunge of CLo is originally zero, then steepens to a maximum of 21°, returning to the horizontal with a different trend. The structural movement paths for lineations and poles to SF and SG are illustrated in Figure 16B and the variations in plunges for these lineations are graphed against positions of SF (Fig. 17B).

Conclusions: For the case with SF rotating about a constant strike direction (Fig. 16A) the resultant cleavage planes at first rotate slowly so that there is only a small change in strike and dip. On further rotation each subsequent change in dip of 10° for SF makes a noticeable rotation in the strike for SG. When the dip of SF changes from 80° to 90° there is a swing in strike of 43° from SG_8 to SG_9. Conversely, in the case where both dip and strike of SF are continually changing (Fig. 16B) there is a more pronounced change in the dip of SG but the swing in strike is not as significant as for case A. The differences in strike and dip between adjacent cleavage planes are summarised below:

		SG_{0-1}	SG_{1-2}	SG_{2-3}	SG_{3-4}	SG_{4-5}	SG_{5-6}	SG_{6-7}	SG_{7-8}	SG_{8-9}
A	strike difference	0	½	1	1	2	4	9	19	43
	dip difference	10	10	10	10	10	10	9	7	4
B	strike difference	0	1	2	3	6	7	8	10	-
	dip difference	2	5	7	11	12	12	13	14	14

The theoretical models outlined in this chapter have been developed in response to a need to provide solutions to problems encountered in the field with respect to quantitative descriptions of folds, development of variably plunging fold axes and the form of a commonly encountered "fracture" cleavage.